

PL-TR-96-2128

**RESEARCH INTO ARTIFICIALLY INDUCED
ATMOSPHERIC DISTURBANCES**

**James W. Duff
Fritz Bien**

**Spectral Sciences, Inc.
99 South Bedford Street, #7
Burlington, MA 01803-5169**

30 June 1996

**Final Report
6 May 1993-19 June 1996**

19970516 086

Approved for public release; distribution is unlimited.



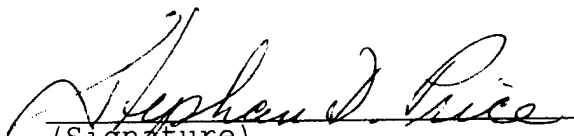
**PHILLIPS LABORATORY
Geophysics Directorate
AIR FORCE MATERIEL COMMAND
HANSCOM AIR FORCE BASE, MA 01731-3010**

DMIC QUALITY INSPECTED 3

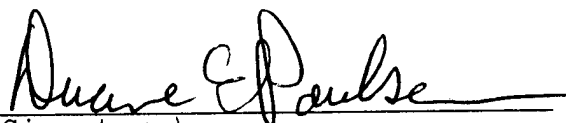
"This technical report has been reviewed and is approved for publication"


(Signature)

Dr. Duane E. Paulsen
Contract Manager


(Signature)

DR. Stephen Price
Branch Chief


(Signature)

Dr. Duane E. Paulsen
Deputy Director
Optical Environment Division
Phillips Laboratory

This report has been reviewed by the ESC Public Affairs Office (PA) and is releasable to the National Technical Information Service (NTIS).

Qualified requestors may obtain additional copies from the Defense Technical Information Center (DTIC). All others should apply to the National Technical Information Service (NTIS).

If your address has changed, if you wish to be removed from the mailing list, or if the addressee is no longer employed by your organization, please notify PL/IM, 29 Randolph Road, Hanscom AFB, MA 01731-3010. This will assist us in maintaining a current mailing list.

Do not return copies of this report unless contractual obligations or notices on a specific document requires that it be returned.

REPORT DOCUMENTATION PAGE

*Form Approved
OMB No. 0704-0188*

Public reporting burden for this collection of information is estimated to average 1 hour per response, including the time for reviewing instructions, searching existing data sources, gathering and maintaining the data needed, and completing and reviewing the collection of information. Send comments regarding this burden estimate or any other aspect of this collection of information, including suggestions for reducing this burden, to Washington Headquarters Services, Directorate for Information Operations and Reports, 1215 Jefferson Davis Highway, Suite 1204, Arlington, VA 22202-4302, and to the Office of Management and Budget, Paperwork Reduction Project (0704-0188), Washington, DC 20503.

1. AGENCY USE ONLY (<i>Leave Blank</i>)	2. REPORT DATE 30 June 1996	3. REPORT TYPE AND DATES COVERED Final Report, 6 May 1993-19 June 1996
---	--------------------------------	---

4. TITLE AND SUBTITLE Research into Artificially Induced Atmospheric Disturbances	5. FUNDING NUMBERS C - F19628-93-C-0052 PE - 62601F PR - S322 TA - GG WU - BE
--	--

6. AUTHOR(S) James W. Duff and Fritz Bien	
--	--

7. PERFORMING ORGANIZATION NAME(S) AND ADDRESS(ES) Spectral Sciences, Inc. 99 South Bedford Street, #7 Burlington, MA 01803-5169	8. PERFORMING ORGANIZATION REPORT NUMBER SSI-TR-279
---	--

9. SPONSORING/MONITORING AGENCY NAME(S) AND ADDRESS(ES) Phillips Laboratory 29 Randolph Road Hanscom AFB, MA 01731-3010 Contract Manager: Duane Paulsen/GPOB	10. SPONSORING/MONITORING AGENCY REPORT NUMBER PL-TR-96-2128
--	---

11. SUPPLEMENTARY NOTES

12a. DISTRIBUTION/AVAILABILITY STATEMENT Approved for public release: distribution is unlimited.	12b. DISTRIBUTION CODE
---	------------------------

13. ABSTRACT (*Maximum 200 words*)
A detailed chemical kinetics model describing the interaction of an electron beam with the atmosphere is used to investigate N(⁴S), N(²D) and N(²P) formation and the subsequent reaction of metastable N atoms with O₂ on NO formation and emission during the EXCEDE III artificial auroral experiment. Of particular significance is the result that rotationally hot NO can be explained by the reaction of nonthermal N(⁴S) atoms with O₂. The rate constants and vibrational distributions for rotationally hot NO are obtained from extensive quasiclassical trajectory calculations for N(⁴S)+O₂ reaction using realistic *ab initio* potential energy surfaces. This analysis provides the first quantitative evidence of the importance of hyperthermal N(⁴S) and N(²D) atoms in the formation of vibrationally and rotationally excited NO. Excellent agreement between the chemical kinetics model developed for EXCEDE and the NO vibrational populations derived from the interferometer data is obtained under conditions of thermalization of nitrogen atoms (i.e., at 103 km under maximum dose conditions). Analysis of vibrational populations from the interferometer under other conditions indicate that hyperthermal N(²D) atoms may also play an important role in NO formation or an additional mechanism for hot NO formation is necessary.

14. SUBJECT TERMS artificial aurora nonthermal nitrogen atoms NO quasiclassical trajectory chemical kinetics vibrational/rotational	15. NUMBER OF PAGES 56
	16. PRICE CODE N/A

17. SECURITY CLASSIFICATION OF REPORT UNCLASSIFIED	18. SECURITY CLASSIFICATION OF THIS PAGE UNCLASSIFIED	19. SECURITY CLASSIFICATION OF ABSTRACT UNCLASSIFIED	20. LIMITATION OF ABSTRACT SAR
---	--	---	-----------------------------------

TABLE OF CONTENTS

<u>Section</u>	<u>Page</u>
1. INTRODUCTION	1
2. ANALYSIS OF N(² D) AND N(² P) EMISSIONS	3
2.1 Measurement of Metastable N(² D) and N(² P)	4
2.1.1 N(² D)	4
2.1.2 N(² P)	4
2.2 Chemical Kinetics Model	4
2.3 Comparison of Data with The Kinetics Model	12
2.4 Summary	16
3. QUASICLASSICAL TRAJECTORY STUDY OF THE TRANSLATIONAL ENERGY DEPENDENCE OF THE N(⁴ S) + O ₂ (X ³ Σ) → NO(X ² Π) + O(³ P) REACTION	17
3.1 Introduction	17
3.2 Potential Energy Surfaces	19
3.3 Classical Trajectory Methodology	25
3.4 Results and Discussion	26
3.4.1 Thermal rate constants	26
3.4.2 Energy Dependent Cross Sections	28
3.4.3 Product Energy Deposition	28
3.5 Summary	34
4. EVIDENCE FOR NO FORMATION FROM HYPERTHERMAL N(⁴ S) ATOMS IN AN ARTIFICIAL AURORAL EXPERIMENT	35
4.1 Introduction	35
4.2 Chemical Kinetics Model	35
4.3 Summary	40
5. SUMMARY	42
6. REFERENCES	44

LIST OF FIGURES

<u>Figure</u>	<u>Page</u>
1. Major Processes for the Production Rate of N(² D) at 115 km.	10
2. Major Processes for the Destruction Rate of N(² D) at 115 km.	10
3. Major Processes for the Production Rate of N(² P) at 115 km.	11
4. Major Processes for the Destruction Rate of N(² P) at 115 km.	11
5. Total Number of Ion Pairs Along the Line-of-Sight as a Function of Mission Elapsed Time for the EXCEDE III Experiment.	14

LIST OF FIGURES (Continued)

<u>Figure</u>	<u>Page</u>
6. Calculated Dose Time as a Function of Mission Elapsed Time for the EXCEDE III Experiment.	14
7. Comparison of the Time Dependence of the Calculated $N(^2D)$ Column Density (o) with the 5200 Å Photometer Data (●).	15
8. Comparison of the Calculated Time Dependence of the $N(^2P)$ Column Density (o) with the 3466 Å Spectrometer Data (●).	15
9. Contour Plot of the NO_2 $^2A'$ Potential Energy Surface at a NOO Bond Angle of 110° . The Contour Values in eV Are 3(1), 2(2), 1(3), 0.3(4), 0.0(5), -0.5(6), and -1(7) Relative to the $N(^4S) + O_2$ Asymptote.	24
10. Contour Plot of the NO_2 $^4A'$ Potential Energy Surface at a NOO Bond Angle of 110° . The Contour Values in eV are 3(1), 2(2), 1(3), 0.5(4), 0.0(5), -0.5(6), and -1(7) Relative to the $N(^4S) + O_2$ Asymptote.	24
11. Bending Potentials of the $^2A'$ and $^4A'$ Surfaces in the Region of the Saddle Point. The Solid Lines are the Analytical Fits Using Equation (1) and Filled Symbols are the Adjusted <i>ab initio</i> Points.	25
12. Comparison of the Experimental (—) and QCT(—●—) Thermal Reaction Rate Constants as a Function of Temperature.	27
13. Contributions of the $^2A'$ and $^4A'$ Potential Energy Surfaces to the Thermal Rate Constant.	27
14. Contribution of the QCT Cross Sections for the $^2A'$ and $^4A'$ Potential Energy Surfaces to the Total Cross Section as a Function of the Initial Relative Translational Energy.	29
15. NO Vibrational Distribution as a Function of the Final Vibrational Quantum Number for Initial Relative Translational Energies of 0.5 and 1.5 eV.	29
16. Contribution of the $^2A'$ and $^4A'$ Potential Energy Surfaces to the NO Vibrational Distribution as a Function of the Final Vibrational Quantum Number at an Initial Relative Translational Energy of 1.5 eV.	30

LIST OF FIGURES (Continued)

<u>Figure</u>		<u>Page</u>
17.	NO Rotational Distribution as a Function of the Final Rotational Quantum Number for Initial Relative Translational Energies of 0.5 and 1.5 eV. The Solid Lines Correspond to Boltzmann Distributions at Rotational Temperatures of 4000 K and 10000 K.	32
18.	NO Rotational Distribution as a Function of Final Rotational Quantum Number for Several Final Vibrational Quantum Numbers at an Initial Relative Translational Energy of 1.5 eV.	32
19.	The Average Rotational Quantum Number as a Function of the Final Vibrational Quantum Number at Initial Translational Energies of 0.5 and 1.5 eV.	33
20.	The Fraction of Total Energy in Translation, Vibration, and Rotation for the Reaction Products as a Function of Initial Relative Translational Energy.	33
21.	Comparison of the NO Vibrational Populations for the Rotationally hot Component Derived from the Interferometer Data at an Altitude of 103 km During Upleg with the EXCEDE Kinetic Model Using the N*(⁴ S) + O ₂ Mechanism.	39
22.	Same as Figure 21 Except for an Altitude of 115 km (apogee).	39

LIST OF TABLES

<u>Table</u>		<u>Page</u>
1.	Parameters for The Diatomic extended-Rydberg Potentials	21
2.	Three Body Parameters for the NO ₂ ² A' and ⁴ A' Potential Energy Surfaces	23

1. INTRODUCTION

The goal of EXCEDE III is to provide a validated data base which can be used to assess chemical kinetic mechanisms in order to reduce the uncertainties in the predictions of the effects of nuclear events on atmospheric radiance. Analyzed data from EXCEDE III will help identify and predict optical signatures from the high-altitude detonation of a nuclear device. To this end, the reaction of electrons with the natural, quiescent atmosphere resulting from dosing by energetic electrons is investigated. A beam of electrons having a nominal initial energy of 2.6 keV was injected into the upper atmosphere between 80 and 115 km. Optical instruments viewed the interaction of these electrons with the atmosphere from both onboard the electron accelerator module and from offboard platforms. Measurements were made of both the electron input and the resultant atmospheric response. The data contains information necessary to characterize the atmosphere before, during, and after the injection of energetic electrons.

The dose rates achieved by EXCEDE III, on the order of 10^{11} cm⁻³ at 110 km, approach the dose range of high altitude nuclear scenarios. The infrared signatures from this dose should be scalable to nuclear code calculations, though only a portion of the phenomenology is applicable. Current uncertainties in the phenomenological models based on reaction rate coefficients and calculated electron concentrations that affect infrared emissions are thought to lie within a factor of 2 or 3 in the best known situations and much worse in many other cases. Although production rates of known species can be quantified in laboratory experiments, the total production of IR active species is not currently available. It is important, then, to verify this degree of confidence by providing a controlled electron dose experiment which will provide an atmospheric database to which these computer models can be compared.

Of particular importance for system applications is validation of both the emission rate and the mechanisms of formation of important infrared radiators in the nuclear disturbed atmosphere. Radiation in spectral regions which normally form atmospheric windows would mean that these windows are not available during a nuclear disturbance. The particular radiating species has an important effect on the design of a system. Species of interest in this context are CO₂ (ν_2 and ν_3), NO ($\Delta v = 1$ and $\Delta v = 2$), CO, O₃, and other oxides of nitrogen

such as N_2O and NO_2 . Emissions from ions, such as NO^+ , could mean geomagnetically formed striations for a satellite system. Unknown or disputed reaction rates include the quenching of precursor species such as $N(^2D)$ by electrons, fractional yields of species such as $N(^2P)$ and $N_2(A)$, effects of these species in the disturbed atmosphere, and creation mechanisms for species such as highly rotationally excited NO , O_3 , and N_2O . Emissions due to very high rotation levels which are not quenched in the field experiment may have a great impact on the atmospheric bandpasses where current surveillance instruments are being designed.

This report describes the investigation of NO emission observed during EXCEDE III performed under Contract No. F19628-93-C-0052. To understand the NO formation mechanisms, it is important to characterize the formation of the N atom precursors thought to be the dominant source of NO . In particular, the reactions of $N(^4S)$, $N(^2D)$, and $N(^2P)$ with O_2 are considered in some detail. To this end, Section 2 describes the chemical kinetics model and a comparison of the predicted $N(^2D)$ and $N(^2P)$ column densities to those derived from the 5200 Å photometer and the visible spectrometer. Section 3 reports the use of quasiclassical trajectories to determine the energy dependent reaction rate constant and $NO(v,J)$ product distributions for the $N(^4S)+O_2$ reaction, which has been proposed as the mechanism for rotationally hot NO formation. The predicted NO populations using the N atom number densities from the chemical kinetics model and the known reaction rate constants for the $N(^2D)+O_2$ and $N(^2P)+O_2$ reactions and calculated rate constants described in Section 2 are compared with the rotationally thermal and hot components of the measured NO column densities in Section 3. A brief summary is given in Section 4.

2. ANALYSIS OF N(²D) AND N(²P) EMISSIONS

The primary source of NO emissions in an aurorally enhanced upper atmosphere is through odd-nitrogen chemiluminescent reactions involving N(⁴S), N(²D), and N(²P). Recent papers speculating on the creation of the NO hot bands have identified high energy nitrogen atoms as the source of these emissions. One of the goals of the EXCEDE III measurement program, which has been described previously,⁽¹⁾ is to understand the electron-beam induced infrared fluorescence resulting from chemical reactions and energy transfer processes. To characterize the relative importance of the N atom precursors in NO formation, the N(²D) and N(²P) emissions have been measured in EXCEDE III. These measurements are compared to a chemical kinetics model which is tested for consistency by using supporting measurements, such as electron deposition, NO chemiluminescence, and N₂ second positive (2P) emissions. The atomic nitrogen formed when an energetic electron interacts with the atmosphere determines not only how much NO is formed, but also the spectral distribution of the chemiluminescence. The relative production of these atoms in a electron excited atmosphere has been measured under controlled conditions in EXCEDE III. Simultaneous measurements of the ²P → ⁴S, ²D → ⁴S, and N₂⁺ first negative (1N) bands have been performed during this experiment. A carefully controlled electron beam dosing profile gave a direct measure of the odd nitrogen production rates as a function of electron injection. The energy deposition profile was measured using 3914 Å emission, and is well represented by a generalized Gaussian function.⁽²⁾ Since the exact mission profile was known, the emissions within the field-of-view of each detector could be compared with the chemical kinetics responsible for the nitrogen formation. This report presents an analysis of the nitrogen atoms produced in its two lowest metastable excited states and predicts the amount of N(⁴S) formed based on branching ratios reported in the literature.

The instruments used to obtain the N atom concentrations consisted of a visible spectrometer for N(²P), and dedicated photometer for N(²D). A second photometer, looking at N₂⁺ 1N, was boresighted with each of these instruments. Since several different instruments were used for these measurements, they are described separately in the sections below. In the following sections, we present the measurement of N(²D) and N(²P), the modeled concentrations based on the observed N₂⁺ (0,0) 1N emissions, and finally a discussion on the

comparison.

2.1 Measurement of Metastable N(²D) and N(²P)

2.1.1 N(²D)

The N(²D) emission was measured by a filter photometer with a center wavelength at 5200 Å and a full width at half maximum (FWHM) of 6.06 Å. The field-of-view (FOV) of the photometer was nominally 6° and was pointed 18° into the afterglow. Data were collected at a sample rate of 750 Hz. In order to correct for possible interfering emission, such as the 0-3 band of the N₂⁺ 1N series at 5228 Å or the Herzberg bands of O₂, an additional photometer with a center wavelength at 5228 Å with a FWHM of 5.79 Å was co-aligned with the 5200 Å photometer.

2.1.2 N(²P)

The measurement of N(²P) produced in EXCEDE III was made by measuring its relative intensity to known features using a visible spectrometer. A more detailed description of this instrument is reported by Reider et al.⁽²⁾ This instrument had a spectral scan time of 2.8 s. Since alternating scans used a neutral density filter (OD = 2) to extend the instrument dynamic range, one 3466 Å measurement was made every 5.6 s. This time, convolved with beam-on times of 7.1 s, limited the number of N(²P) scans to 15, 6 on upleg, one at apogee, and 8 on the downleg. The feature at 3466 Å is in the region of the spectrum where the N₂⁺ and N₂ 2nd Positive bands are located. In fact, the Δv = 1 series of N₂(2+) has a band in near coincidence with N(²P), at 3468 Å.

2.2 Chemical Kinetics Model

The most important infrared emitters in an electron-dosed atmosphere include NO, CO₂, NO⁺, CO, and O₃. A general chemical kinetics model has been developed to describe the chemical and collisional processes occurring during the dosing of the atmosphere with an energetic electron beam. The model uses a finite rate approach to the modeling of the generation of energy dependent secondary electrons, vibrationally and electronically excited species resulting from collisional energy transfer and chemiluminescent reactions. In

particular, time and energy dependent rate equations are solved for arbitrary electron beam dosing to obtain species number densities as a function of time. The secondary electron spectrum is treated by setting up an energy grid (histogram) at sufficiently high resolution to accurately solve electron-molecule and electron-electron interactions. Time-dependent rate equations are then solved for each energy bin. Chemical and collisional processes for individual vibrational states are treated explicitly. Self-relaxation of secondary electrons, which is important due to the high electron beam fluxes produced in the EXCEDE experiment, has been treated by solving the time-dependent Fokker-Planck equation.^(3,4) In the remainder of this section, the detailed chemical and collisional processes influencing the production and destruction of metastable nitrogen atoms is discussed in some detail.

When electrons interact with the natural atmosphere, dissociation and ionization form odd nitrogen in the form of $N(^2P)$, $N(^2D)$, and $N(^4S)$. Collisions between these species and O_2 create NO.⁽⁵⁾ This production rate is in turn found to be dependent on the ratio of $N(^2D)$ to $N(^4S)$ formed in the interaction of electrons and N_2 . Nitric oxide is currently thought to be produced primarily by the reaction of $N(^2D)$ with O_2



where the reaction rate constant⁽⁶⁾ and NO vibrational distribution^(7,8) are well established at room temperature. Recent laboratory studies⁽⁸⁾ have indicated that $N(^2P)$ produces NO in high vibrational and rotational states

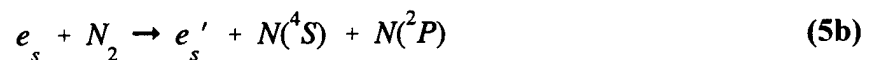
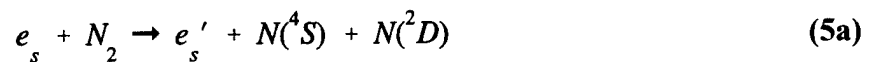
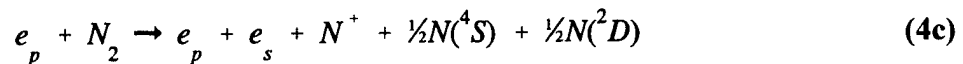
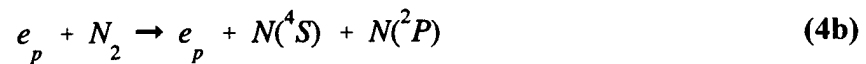
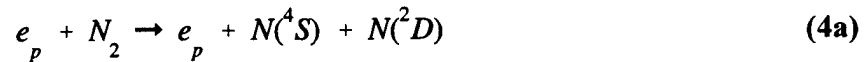


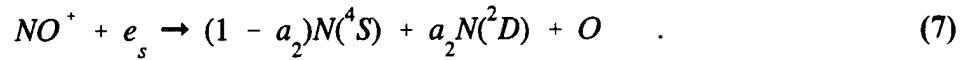
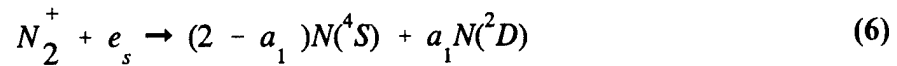
with a rate constant a factor of 2 smaller than Reaction (1).⁽⁶⁾ Furthermore, it has been suggested by Sharma et al.,⁽⁹⁾ that translationally hot $N(^4S)$ atoms⁽¹⁰⁾ may be a significant source of rotationally hot NO in the thermosphere



Although the reaction rate constant and the final vibrational-rotational distribution at high translational energies have not been measured, recent calculations by Duff et al.,⁽¹¹⁾ have established realistic rate constants and NO vibrational-rotational distributions for Reaction (3). A realistic description of the formation and emission of NO in the ambient or auroral atmosphere requires a detailed treatment of nitrogen atom chemistry.

Nitrogen atoms are produced by several major processes; dissociation of N₂ by the primary electrons (e_p) in the electron beam, Reaction (4), dissociation of N₂ by the secondary electrons (e_s) produced by ionization of atmospheric species by the electron beam, Reaction (5), and recombination reactions of the primary ionic products with secondary electrons, Reactions (6) and (7),



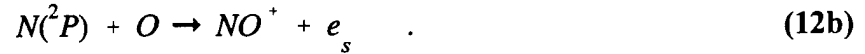


The total production rate of N atoms from Reactions (4a) and (4b) is assumed to be $1.5P(N_2^+)$,^(12, 13) where $P(N_2^+)$ is the N_2^+ production rate, with the relative formation rate of $N(^2D)$ and $N(^2P)$ in the ratio 0.52:0.48.⁽¹⁴⁾ For dissociative ionization by primary electrons, Reaction (4c), the production rate is $0.50P(N_2^+)$.⁽¹⁵⁾ Thus, the total production rate of N atoms from Reaction (4) is $2P(N_2^+)$, or 1.24 N atoms/ion pair, in good agreement with the results of Porter et al.,⁽¹²⁾ and Rusch et al.,⁽¹³⁾ The cross sections for dissociation of N_2 by low energy secondary electrons, Reaction (5), are based on the analysis of Zipf et al.,⁽¹⁴⁾ The rate constants for the recombination of N_2^+ and NO^+ ions with secondary electrons, Reactions (6) and (7), have been measured by Mehr and Biondi⁽¹⁶⁾ and Alge et al.,⁽¹⁷⁾ respectively. The associated branching ratios for the N_2^+ and NO^+ recombination reactions are $a_1 = 1.86$ ⁽¹⁸⁾ and $a_2 = 0.76$.⁽¹⁹⁾ In addition to Reactions (4) through (7), minor sources of $N(^2D)$ considered are the charge exchange reactions of N_2^+ with O ⁽²⁰⁾ and N^+ with O_2 ^(21,22)

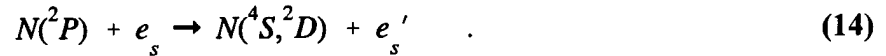


Nitrogen atoms are also subject to quenching by other species which compete with Reactions (1) and (2) in the production of NO





The quenching rates of Reactions (10) - (12)^(6,23) are slow on the time scale of the EXCEDE III measurements in comparison to the efficient quenching of N(²D) and N(²P) by secondary electrons,⁽²⁴⁾ which results from the large density of secondary electrons created by the ionization rates achieved in the experiment



In addition to collisional quenching, N(²D) and N(²P) can undergo radiative relaxation



Since the N atom production from direct electron impact excitation and recombination reactions depends on the low energy secondary electron spectra, it is important that the histogram treatment retain the major features of the secondary electron spectra. Secondary electrons are formed via collisional ionization of M(= N₂, O₂, or O)



The nascent secondary electron energy distribution resulting from (17) is that given by Opal et al.,⁽²⁵⁾ which then relaxes by collisions with major species



and



as well as electron-electron collisions



where the primes refer to secondary electrons in different energy bins. The ion production rates from Reaction (17) are related to the ion pair production rate via the expressions given by Rees and Jones.⁽²⁶⁾ The rate constants for Reactions (18) and (19) were taken from the reviews of Itikawa et al.,^(27,28) for N₂ and O₂ and Itikawa and Ichimura⁽²⁹⁾ for O.

One of the most important inputs to the model is the electron beam characteristics, i.e., the radial profile of the ion-pair production rate. Historically, the electron deposition information has been deduced from the N₂⁺ first negative 3914 Å emission, where it is assumed that there are 14.1 N₂⁺ ions created for each 3914 Å photon.⁽²⁶⁾ Therefore, the beam ion pair production rate profiles used in the current model are based on an analysis of the 3914 Å data by Rieder et al.,⁽²⁾ The N₂⁺ production rate, $P(N_2^+)$, is related to the total ion pair production rate, P_{ion} , by

$$P(N_2^+) = \frac{0.92[N_2]}{1.15[N_2] + 1.5[O_2] + 0.56[O]} P_{ion} \quad (21)$$

where the numerical factors in the expression represent the relative ionization cross sections for N_2 , O_2 , and O .⁽²⁶⁾ Using the atmospheric profile appropriate for the EXCEDE III experiment, the relative production rate of N_2^+ ions is approximately independent of altitude (ranging from 0.60 at 95 km to 0.62 at 115 km).

Representative predictions of the production and destruction rates for $N(^2D)$ and $N(^2P)$ are presented in Figures 1 through 4 for an altitude of 115 km. The electron beam ion pair

production rate is represented by a generalized Gaussian function⁽²⁾ with a peak ion pair production rate of 1.6×10^{11} ion pairs/cm³-s and a full width at half maximum of 14 ms.

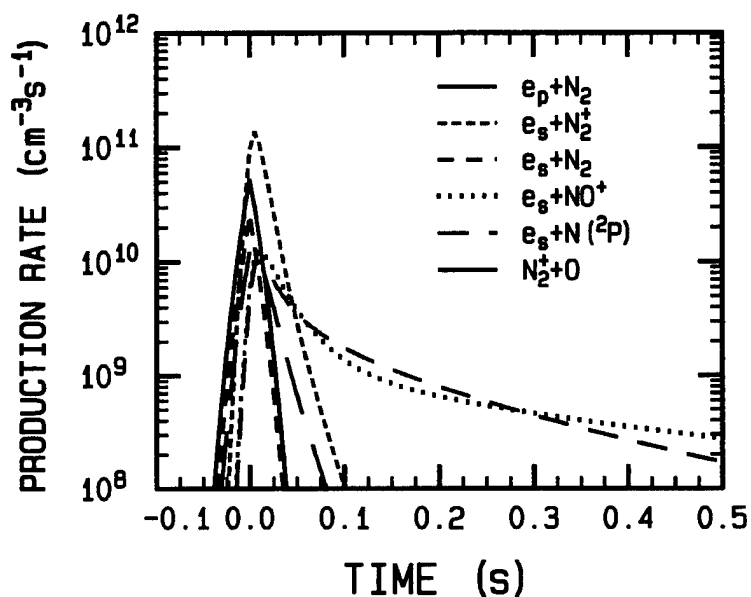


Figure 1. Major Processes for the Production Rate of N(²D) at 115 km.

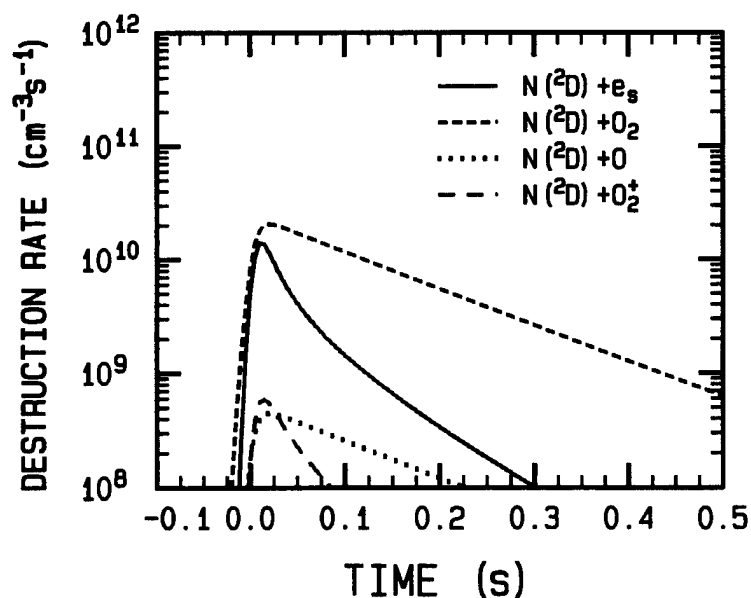


Figure 2. Major Processes for the Destruction Rate of N(²D) at 115 km.

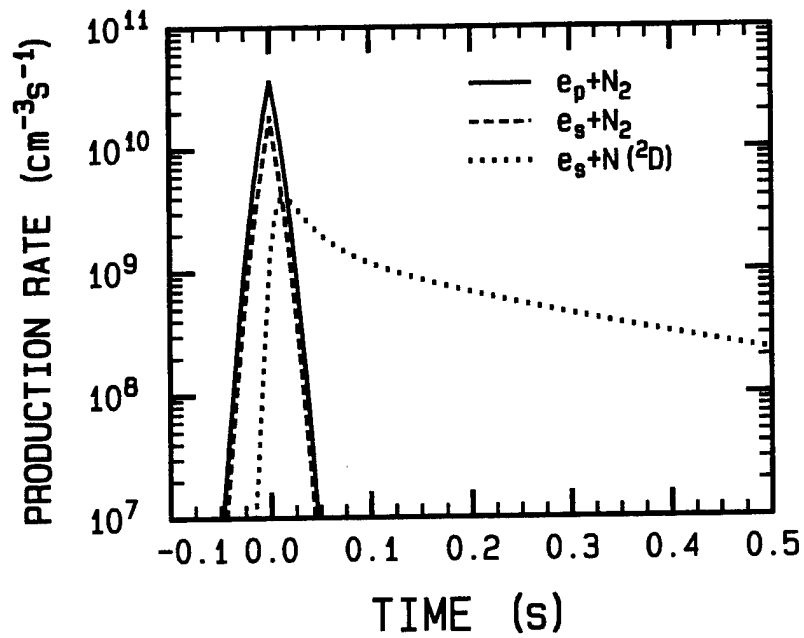


Figure 3. Major Processes for the Production Rate of $N(^2P)$ at 115 km.

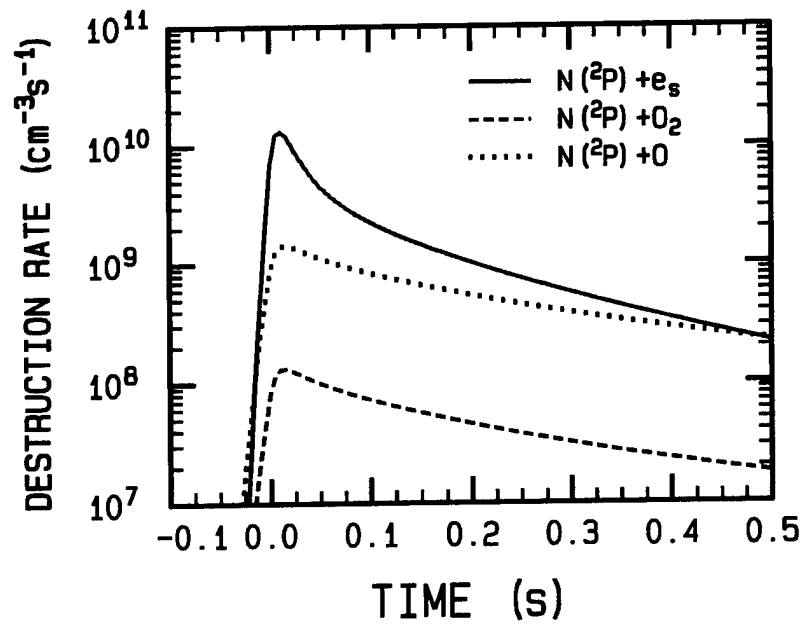


Figure 4. Major Processes for the Destruction Rate of $N(^2P)$ at 115 km.

2.3 Comparison of Data with The Kinetics Model

The chemical kinetics mechanism described previously has been incorporated into the EXCEDE chemical kinetics data base. The resultant data base contains 6703 reactions and energy transfer processes. The chemical kinetics equations are integrated using Gear's method for stiff differential equations⁽³⁰⁾ as a function of time for a specified electron beam ion-pair production rate and altitude. The atmospheric profiles for N₂, O₂, and O were obtained from the MSISE-90 atmospheric model⁽³¹⁾ for the geophysical parameters appropriate to the EXCEDE III experiment.

The geometry of the flight experiment, which includes the trajectory of the gun module, the geomagnetic azimuth and dip angles, and the viewing geometry of the 3466 Å visible spectrometer and 5200 Å photometer on the sensor module, has also been incorporated in the model. The time-dependent nitrogen atom number densities are integrated along the instrument line-of-sight to obtain the column densities as a function of time. The resultant column densities are then integrated over the 6° FOV of the instruments for comparisons with the column densities obtained from 3466 Å and 5200 Å data.

To illustrate the electron beam energy deposition throughout the EXCEDE flight, the total number of ion pairs produced by the electron beam is shown as a function of mission elapsed time (or altitude) in Figure 5. The number of ion pairs was obtained by integrating the observed 3914 Å scanning photometer data along the component of gun vehicle velocity vector perpendicular to the magnetic field lines. The maximum number of ion pairs are created near 102 km on upleg, where, due to the near zero velocity across the field lines, the atmosphere is dosed for nearly 0.5 seconds. The average electron-deposition time, which is simply the root mean square electron beam diameter divided by the velocity across the field lines, is shown in Figure 6. As altitude increases, the number of ion pairs produced decreases due to the shorter deposition times (i.e., the velocity across the field lines is increasing with altitude), see Figure 6. On downleg, the number of ion pairs again increases as altitude decreases, although the total number of ion pairs created is substantially less on downleg than on upleg. This effect is due to the atmosphere being irradiated by the electron beam for times up to a factor of 50 longer on upleg than on downleg, again as shown in Figure 6. The two

data points at approximately 114 and 113 km are about 75% of the expected beam power output due to beam load faults.

The comparisons of the $N(^2D)$ and $N(^2P)$ column densities obtained from the 5200 Å and 3466 Å data with the model predictions which have been integrated along the line-of-sight and integrated over the sensor field-of-view are shown in Figures 7 and 8, respectively. The agreement between the model predictions and data is excellent on both upleg and downleg for the $N(^2D)$ measurements. The altitude dependence of the $N(^2D)$ column density measurement, which looks 18° into the afterglow, is controlled by quenching of $N(^2D)$ by secondary electrons with increasing importance of the $N(^2D)+O_2$ reaction near 100 km. On upleg, the largest discrepancy between the model and data is at 109 and 111 km on upleg, which is not understood, although it is likely related to the uncertainty in the secondary electron quenching rate of $N(^2D)$. The differences between upleg and downleg $N(^2D)$ column densities simply reflect the differences the ion pair production rate, although the ratio of upleg to downleg $N(^2D)$ column densities is less sensitive to ion pair production rate due to the significant quenching of $N(^2D)$ and the fact that the primary production process for $N(^2D)$ is recombination of secondary electrons with N_2^+ . The production rate of $N(^2D)$ from recombination roughly increases as the square root of the ion pair production rate.

The comparison of the model predictions with the 3466 Å data shown in Figure 8 indicate that the $N(^2P)$ chemistry is not as well established as the $N(^2D)$ chemistry. This comparison would indicate that the assumed production rate of 0.22 $N(^2P)$ /ion pair used in Reaction (4b) is approximately a factor of 2 low. Since the total production rate of N atoms is fairly well established, increasing the rate for Reaction (4b) by a factor of 2 would imply that only $N(^2P)$ is produced by dissociation of N_2 by primary electrons. Such a modification in the $N(^2D)/N(^2P)$ relative production rate from Reaction (4) would not significantly alter the excellent agreement between the predictions and the 5200 Å data since the major production mechanism for $N(^2D)$ is the recombination of N_2^+ with secondary electrons, Reaction (6), as shown in Figure 1. Furthermore, the increase in $N(^2P)$ would provide more $N(^2D)$ due to the increased quenching rate from Reaction (14).

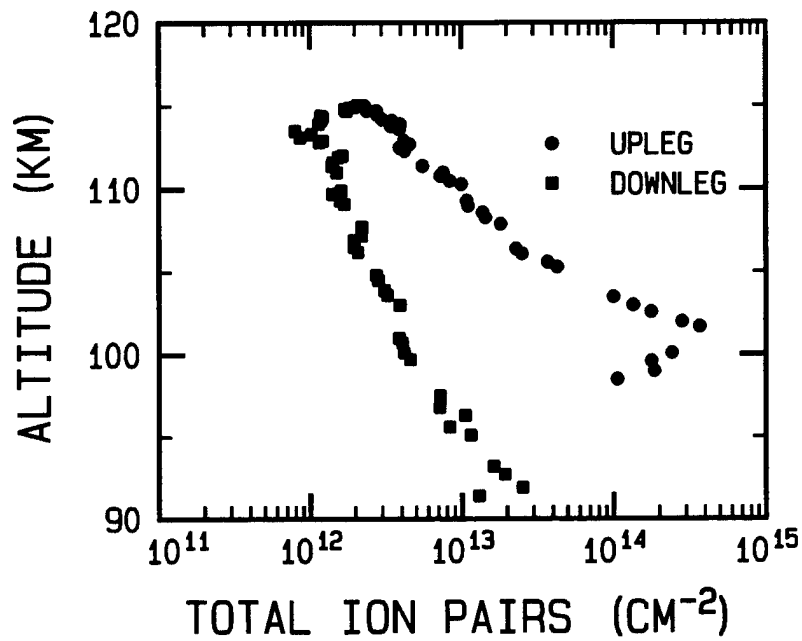


Figure 5. Total Number of Ion Pairs Along the Line-of-Sight as a Function of Mission Elapsed Time for the EXCEDE III Experiment.

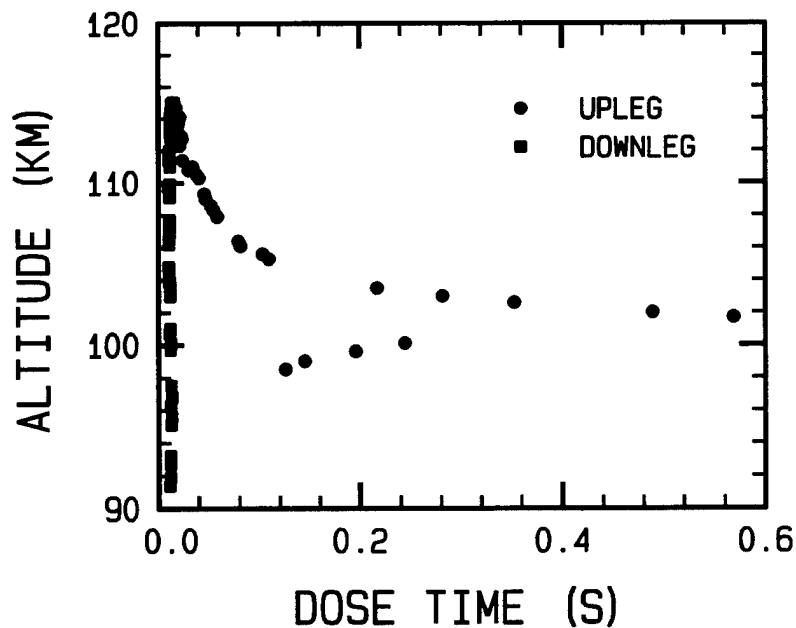


Figure 6. Calculated Dose Time as a Function of Mission Elapsed Time for the EXCEDE III Experiment.

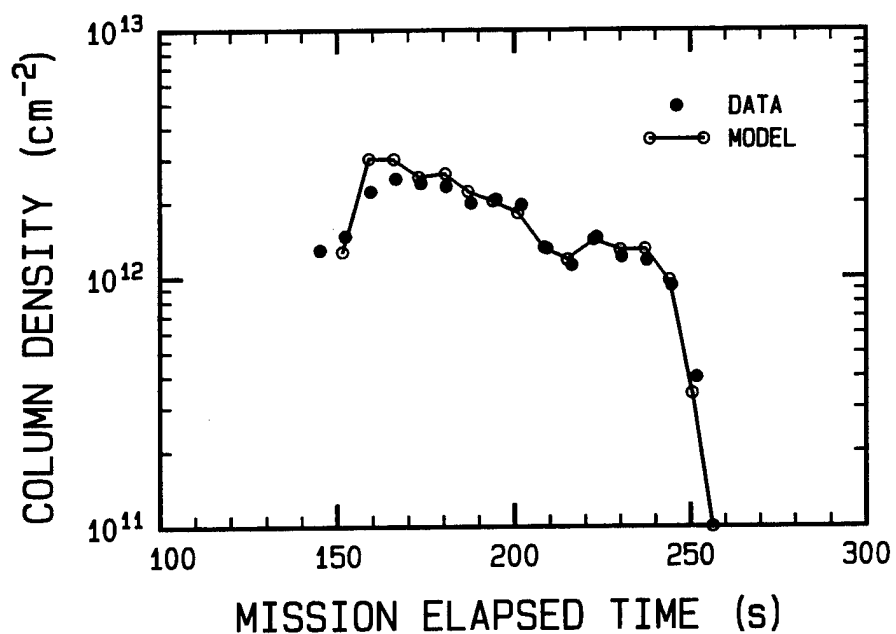


Figure 7. Comparison of the Time Dependence of the Calculated N(²D) Column Density (o) with the 5200 Å Photometer Data (●).

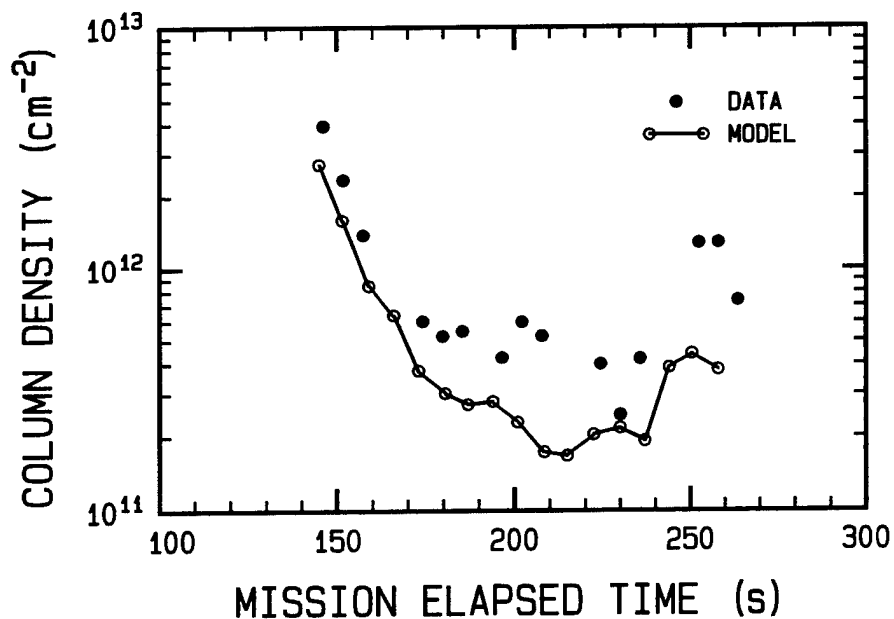


Figure 8. Comparison of the Calculated Time Dependence of the N(²P) Column Density (o) with the 3466 Å Spectrometer Data (●).

2.4 Summary

The EXCEDE III experiment has provided quantitative characterization of the $N(^2D)$ 5200 Å and $N(^2P)$ 3466 Å emissions resulting from the irradiation of the lower thermosphere (90 - 115 km) by an intense electron beam. A detailed chemical kinetics model indicates that the $N(^2D)$ emission can be quantitatively explained by assuming accepted production rates of $N(^2D)$ and N_2^+ created by the electron beam dissociation, consistent with previous auroral models. Using the previous estimate of 0.22 $N(^2P)$ per ion pair⁽¹⁴⁾ from electron dissociation of N_2 results in a model prediction which is approximately 50% below the data, in disagreement with previous analyses of $N(^2P)$ auroral and dayglow emission.^(14,32,33) However, it should be recalled that the EXCEDE III measurement of $N(^2P)$ was not made under steady state conditions, which are appropriate to the atmospheric observations. The present analysis would imply that the amount of $N(^2P)$ from N_2 dissociation should be about a factor of 2 greater than previously assumed or an additional source of $N(^2P)$ exists for intense electron beams such as that used in EXCEDE III.

3. QUASICLASSICAL TRAJECTORY STUDY OF THE TRANSLATIONAL ENERGY DEPENDENCE OF THE $N(^4S) + O_2(X^3\Sigma_g^-) \rightarrow NO(X^2\Pi) + O(^3P)$ REACTION

3.1 Introduction

It is recognized that nitric oxide plays an important role in the energy budget and photochemistry of the lower thermosphere. The reactions of metastable nitrogen atoms with molecular oxygen are thought to be the major source of NO chemiluminescence in the thermosphere.⁽⁵⁾ Standard kinetic models of NO formation assumed that the thermal chemistry of $N(^2D)$ is the most significant contributor to NO formation, while the relaxation of $N(^2P)$ to $N(^2D)$ and the reaction of $N(^2P)$ with O_2 make a relatively minor contribution to NO formation in the thermospheric dayglow⁽³³⁾ and aurora.^(14,32) At thermospheric temperatures, the reaction of $N(^4S)$ with O_2 is much slower than Reactions (1) and (2) and, therefore, has not been considered a significant source of NO. However, Solomon⁽³⁴⁾ has suggested that the reaction of translationally hot $N(^4S)$ atoms with O_2 may be an important factor in the formation of NO in the thermosphere. Detailed models involving the solution of the Boltzmann equation for the kinetic description of $N(^4S)$ atoms in the thermosphere have shown the translational energy distribution to be highly nonthermal.^(10, 35-37)

Model predictions by Gérard and coworkers^(10,36) have also shown that the reaction of these nonthermal $N(^4S)$ with O_2 makes a significant contribution to thermospheric NO formation in the daytime. Furthermore, Sharma et al.,⁽⁹⁾ have argued for the importance of the $N(^4S) + O_2$ reaction in recent observations of highly rotationally excited NO vibrational emissions in the dayglow.^(38, 39) Their analysis was based on two recent studies; a quasiclassical trajectory study of ground state $N(^4S) + O_2$ reaction by Gilibert et al.,⁽⁴⁰⁾ indicating that the $N(^4S)$ reaction efficiently produces NO in high ro-vibrational states and the calculated nonthermal thermospheric $N(^4S)$ translational energy distribution.⁽¹⁰⁾ Further evidence showing the importance of Reaction (3) in producing highly rotationally excited NO in the atmosphere has been provided by the analysis of NO emission observed during an artificial auroral experiment in the lower thermosphere.⁽⁴¹⁾ However, Rawlins et al.,⁽⁸⁾ have interpreted the formation of highly rotationally excited NO in laboratory experiments from the

reaction $N(^2D)$, although it has been pointed out by Smith and Ahmadjian⁽³⁸⁾ that the density of $N(^2P)$ is insufficient to account for the atmospheric observations. In order to assess the importance of the $N(^4S) + O_2$ as a source of vibrationally and rotationally excited NO, the reaction rate constant and NO vibrational-rotational distribution must be determined as a function of $N(^4S)$ translational energy.

The present theoretical study uses extensive quasiclassical trajectory(QCT) calculations to determine the reaction rate constant and the nascent NO vibrational-rotational distributions formed by the translationally hot $N(^4S) + O_2$ reaction as a function of $N(^4S)$ translational energy from 0.5 to 2.75 eV. A new analytical fit to the $^2A'$ and $^4A'$ *ab initio* potential energy surfaces of Walch and Jaffe⁽⁴²⁾ is used to predict the reaction attributes of $N(^4S) + O_2$. The reaction attributes have been independently calculated on each potential energy surface and then statistically averaged using the electronic degeneracy factors. The lowest $^2A'$ potential energy surface, which has an estimated activation energy of approximately 0.3 eV,⁽⁴⁰⁾ makes the dominant contribution to the reaction rate for temperatures below 1500 K. Although the $^4A'$ surface, which has an estimated barrier of 0.65 eV,⁽⁴²⁾ does not contribute to the reaction rate for temperatures below 1500 K, it must be considered for the translationally "hot" $N(^4S)$ reaction. The results of this study provide the reaction attributes of $N(^4S) + O_2$ useful for modeling the production of NO from "hot" $N(^4S)$ ^(10, 35-37) and the NO dayglow emission spectra.^(9, 38, 39)

The only experimental data on the $N(^4S) + O_2$ reaction are thermal rate constant measurements,⁽⁴³⁾ which are reliable up to 1500 K, the NO vibrational distribution at room temperature,⁽⁴⁴⁻⁴⁶⁾ and a preliminary study of energy dependence of the NO vibrational-rotational emission using bandpass filters covering the NO fundamental and overtone spectral regions.⁽⁴⁷⁾ No direct experimental measurements of the energy dependence of the reaction cross section, or equally important for thermospheric modeling of NO emission spectra, the disposal of available energy into NO vibration and/or rotation, are currently available. There also is evidence that the measured NO vibrational distributions have undergone vibrational relaxation, and therefore may be colder than the nascent distribution.

There have been two previous quasiclassical trajectory calculations reported for the $N(^4S) + O_2$ reaction. The first study was performed by Jaffe et al.,⁽⁴⁸⁾ using the $^2A'$ and $^4A'$ surfaces mentioned above. However, their study emphasizes the thermal reaction rate constant at high temperatures and, although consistent with experiment, do not provide rate constants as a function of collision energy or final state distributions of the products. The second quasiclassical trajectory study by Gilibert et al.,⁽¹³⁾ only considered the lowest potential energy surface, $^2A'$, and therefore is applicable to thermal collisions below 1500 K or collision energies less than approximately 0.75 eV. More importantly, the fitting of an analytical functional form to the calculated *ab initio* $^2A'$ potential energy surface introduced an artificial barrier of approximately 0.55 eV in the reactant channel, which implies that the calculated threshold for reaction is too high by approximately 0.22 eV. Thermal rate constants calculated using the $^2A'$ PES of Gilibert et al., would result in an activation energy approximately 5 kcal/mole higher than experiment. Recently, Gilibert et al.,⁽⁴⁹⁾ have compared their QCT results with a Reactive Infinite Order Sudden Approximation (R-IOSA) study of the $N(^4S) + O_2$ reaction. The general features of the reaction dynamics obtained from the R-IOSA study are in general agreement with the QCT calculations.

The remainder of this section is organized as follows. Section 3.2 discusses the construction of the potential energy surfaces used to study the reaction of hyperthermal $N(^4S)$ and with O_2 in producing NO. The trajectory calculations are briefly discussed in Section 3.3, while in Section 3.4 results of the chemical dynamic study are presented. A brief summary is given in Section 3.5.

3.2 Potential Energy Surfaces

The reaction of $N(^4S) + O_2(X^3\Sigma_g^-)$ to form $NO(X^2\Pi) + O(^3P)$ is exothermic by 1.38 eV and occurs on two electronic potential energy surfaces of $^2A'$ and $^4A'$ symmetry (neglecting spin-orbit coupling). The electronic degeneracies are such that 4/12 of the $N(^4S) + O_2$ collisions occur on the $^4A'$ surface compared to 2/12 on the ground state $^2A'$ surface. The remaining 6/12 of the collisions occur on the $^6A'$ surface which correlates with the excited state products $NO(a^4\Pi) + O(^3P)$, and is not considered further. An extensive set of *ab initio* quantum mechanical calculations for the $^2A'$ and $^4A'$ potential energy surfaces have been

carried out by Walch and Jaffe⁽⁴²⁾ to characterize the saddle point geometries and to a lesser extent the minimum energy path. Other previous work on the NO₂ system has been discussed in some detail by Gilibert et al.,⁽⁴⁰⁾

The recent *ab initio* calculations of Walch and Jaffe for the ²A' and ⁴A' potential energy surfaces (PES) are used as a basis for the analytical representation of the N(⁴S) + O₂ reaction. Their study involved a total of 66 *ab initio* points for the ²A' surface and 23 for the ⁴A' surface at the complete active space self-consistent field (CASSCF) level followed by multireference contracted configuration interaction (CCI) calculations. An additional 11 points were computed at the ext.CCI level to approximately characterize the minimum energy path and energy release on the ²A' ground state surface. The "best" theoretical estimate of the barrier height for the ²A' surface was felt to be 2 - 3 kcal/mole too high compared with the experimental activation energy. In creating the analytical representation of the PES, the calculated *ab initio* points in the vicinity of the saddle point were adjusted by a constant factor such that the barrier heights for the ²A' and ⁴A' are in agreement with the experimental estimate for the ²A' surface⁽⁴³⁾ and theoretical estimate for the ⁴A' surface.⁽⁴²⁾ The adjusted *ab initio* points were then fit to an analytical representation of the potential energy surface suggested by Sorbie and Murrell(SM)⁽⁵⁰⁾ using a nonlinear least squares method.

The SM analytical form for the PES is given by the sum of two-body diatomic potentials, V⁽²⁾(r), and a three-body term, V₁⁽³⁾,

$$V_{NOO}(r_1, r_2, r_3) = V_{NO}^{(2)}(r_1) + V_{OO}^{(2)}(r_2) + V_{NO}^{(2)}(r_3) + V_1^{(3)}(r_1, r_2, r_3) \quad (22)$$

where r₁, r₂, r₃ are the NO, O₂, NO internuclear distances, respectively. The diatomic potentials are represented by a modified Rydberg potential⁽⁵¹⁾

$$V^{(2)}(r) = -D_e [1 + a_1(r - r_e) + a_2(r - r_e)^2 + a_3(r - r_e)^3] \exp[-a_1(r - r_e)] \quad (23)$$

where D_e is the dissociation energy, r_e is the equilibrium internuclear distance, and (a_1, a_2, a_3) are parameters fit to the RKR potential. The parameters for NO and O₂ given in Table 1 are identical to those used by Gilibert et al.,⁽⁴⁰⁾ The three-body term is a product of a range function,

Table 1. Parameters for The Diatomic extended-Rydberg Potentials.^a

	D_e	r_e	a_1	a_2	a_3
NO($X^2\Pi_{1/2}$)	6.6144	1.1508	5.035	5.151	2.998
O ₂ ($X^3\Sigma_g^-$)	5.2132	1.2075	5.476	7.950	6.341

^aEnergies are given in eV and distances in Ångstroms.

which ensure the correct asymptotic behavior, and a polynomial expressed as a function of internal coordinates

$$V^{(3)}(r_1, r_2, r_3) = V_0 T_1 T_2 T_3 (1 + \sum_{jkl} c_{jkl} s_1^j s_2^k s_3^l) \quad (24)$$

where the internal coordinates are defined

$$s_1 = 1/\sqrt{2}(\rho_1 + \rho_3) \quad (25a)$$

$$s_2 = \rho_2 \quad (25b)$$

$$s_3 = 1/\sqrt{2}(\rho_1 - \rho_3) \quad (25c)$$

with

$$\rho_i = r_i - r_i^o \quad (26)$$

The sum in Equation (24) consists of a polynomial in internal coordinates such that $0 < j + k + l \leq M$, where $M = 4$ for the present case. The range functions, which decay exponentially as $s_i \rightarrow \infty$, are defined in terms of hyperbolic tangents

$$T_i = 1 - \tanh(\gamma_i s_i/2) \quad (27)$$

The three-body potential defined by Equations (24) - (27) requires the determination of 41 parameters, 14 of which vanish due to symmetry, and 3 of which are specified ($r_1^0, r_2^0, r_3^0 = r_1^0$). The remaining 24 parameters are determined by a nonlinear fit to the adjusted *ab initio* points.

Using the original 77 *ab initio* points for the $^2A'$ resulted in an analytical function, which displayed spurious wells and barriers in the entrance channel similar to those found in the fit by Gilibert et al.,⁽⁴⁰⁾ This undesired result was remedied by generating additional points in the $N(^4S) + O_2$ entrance channel assuming that the three body interaction term decreases exponentially as $r_{NO} \rightarrow \infty$. This assumption has no influence on the reaction dynamics, but removes the spurious artifacts in the analytical fit. The parameters (γ_i and c_{jkl}) in Equations (24) and (27) are determined by fitting to the set of adjusted *ab initio* points, augmented with additional points in the entrance channel, with a standard deviation of 0.047 eV for both surfaces. The final parameters for the $^2A'$ and $^4A'$ three-body potential energy surfaces are given in Table 2.

Contour plots of the $^2A'$ and $^4A'$ potential energy surfaces are shown in Figures 9 and 10 for a bond angle, θ_{NOO} , of 110° . The resultant barrier heights of the analytical functions are 0.3 eV and 0.65 eV for the $^2A'$ and $^4A'$ potential energy surfaces, respectively. The saddle point geometry is given by $r_{NO} = 1.921 \text{ \AA}$, $r_{OO} = 1.216 \text{ \AA}$, and $\theta_{NOO} = 111^\circ$ for the $^2A'$ surface and $r_{NO} = 1.813 \text{ \AA}$, $r_{OO} = 1.232 \text{ \AA}$, and $\theta_{NOO} = 107^\circ$ for the $^4A'$, in excellent agreement with the *ab initio* results. The angular dependence of the barrier for both surfaces is also accurately reproduced by the analytical function, as is shown in Figure 11. Both surfaces are characterized by attractive energy release,⁽⁵²⁾ which is typical of surfaces with early barriers in the entrance channel. However, it is apparent from the contour plots that the curvature of the $^4A'$ minimum energy path is smaller than that for the $^2A'$ which would imply that NO vibrational excitation would be more efficient for the $^2A'$ PES.⁽⁵³⁾ It should be noted that although the *ab initio* calculations indicate that the curvature of the minimum energy path for $^4A'$ is smaller than that for the $^2A'$, the location and curvature of the minimum energy path and the energy release were not completely determined for the $^4A'$ in the study of Walch and Jaffe.

Table 2. Three Body Parameters for the NO₂ ²A'' and ⁴A'' Potential Energy Surfaces.^a

	² A''	⁴ A''
V ₀	1.701	1.815
c ₁₀₀	-0.730	-0.372
c ₀₁₀	3.632	3.751
c ₀₀₁	0.0	0.0
c ₂₀₀	1.415	1.239
c ₁₁₀	-2.252	-1.627
c ₁₀₁	0.0	0.0
c ₀₂₀	13.414	15.507
c ₀₁₁	0.0	0.0
c ₀₀₂	-0.235	0.435
c ₃₀₀	-0.393	-0.448
c ₂₁₀	4.710	5.252
c ₂₀₁	0.0	0.0
c ₁₂₀	-1.157	0.743
c ₁₁₁	0.0	0.0
c ₁₀₂	0.840	0.497
c ₀₃₀	44.312	44.236
c ₀₂₁	0.0	0.0
c ₀₁₂	0.662	1.582
c ₀₀₃	0.0	0.0
c ₄₀₀	0.332	0.611
c ₃₁₀	1.202	1.039
c ₃₀₁	0.0	0.0
c ₂₂₀	15.287	8.057
c ₂₁₁	0.0	0.0
c ₂₀₂	-2.611	-0.380
c ₁₃₀	10.539	4.325
c ₁₂₁	0.0	0.0
c ₁₁₂	6.708	9.283
c ₁₀₃	0.0	0.0
c ₀₄₀	73.573	95.293
c ₀₃₁	0.0	0.0
c ₀₂₂	5.567	3.686
c ₀₁₃	0.0	0.0
c ₀₀₄	3.611	2.911
Y ₁	2.579	2.771
Y ₂	7.449	7.763
Y ₃	0.0	0.0
r ₁ ⁰	2.2076	2.2076
r ₂ ⁰	1.2320	1.2320
r ₃ ⁰	2.2076	2.2076

^aEnergies are given in eV and distances in Angstroms.

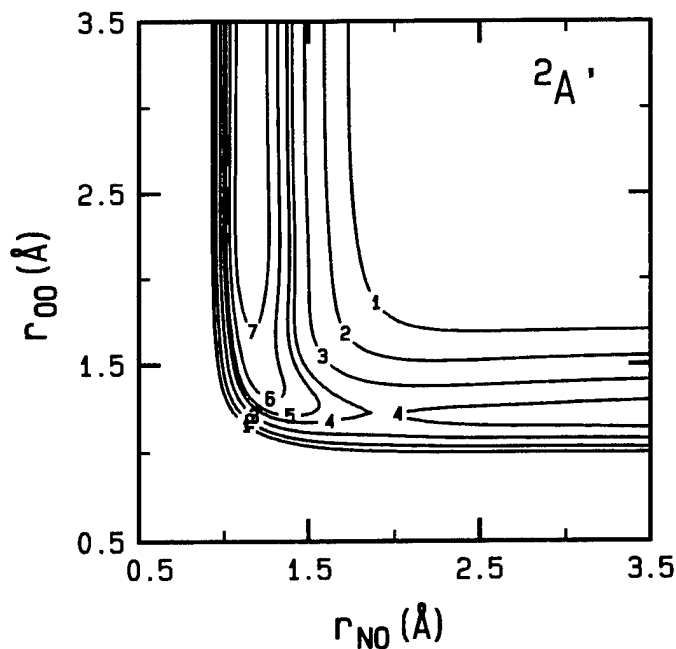


Figure 9. Contour Plot of the NO_2 $^2A'$ Potential Energy Surface at a NOO Bond Angle of 110° . The Contour Values in eV Are 3(1), 2(2), 1(3), 0.3(4), 0.0(5), -0.5(6), and -1(7) Relative to the $\text{N}(^4S) + \text{O}_2$ Asymptote.

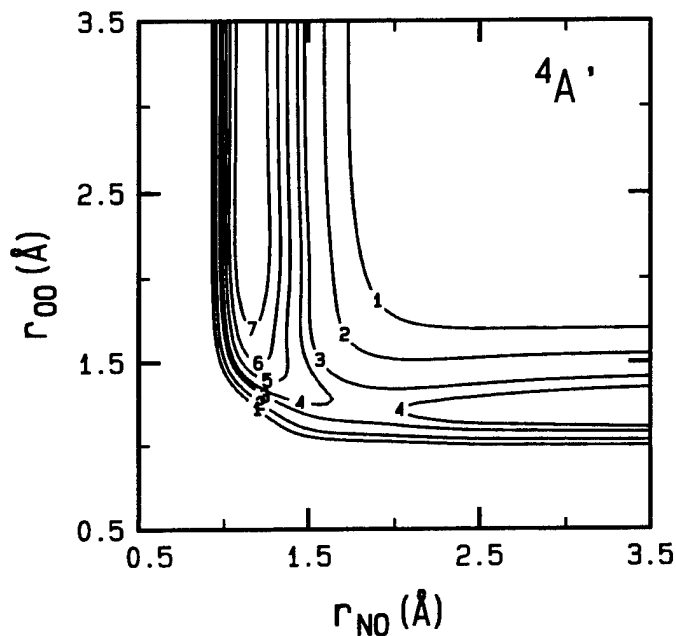


Figure 10. Contour Plot of the NO_2 $^4A'$ Potential Energy Surface at a NOO Bond Angle of 110° . The Contour Values in eV are 3(1), 2(2), 1(3), 0.5(4), 0.0(5), -0.5(6), and -1(7) Relative to the $\text{N}(^4S) + \text{O}_2$ Asymptote.

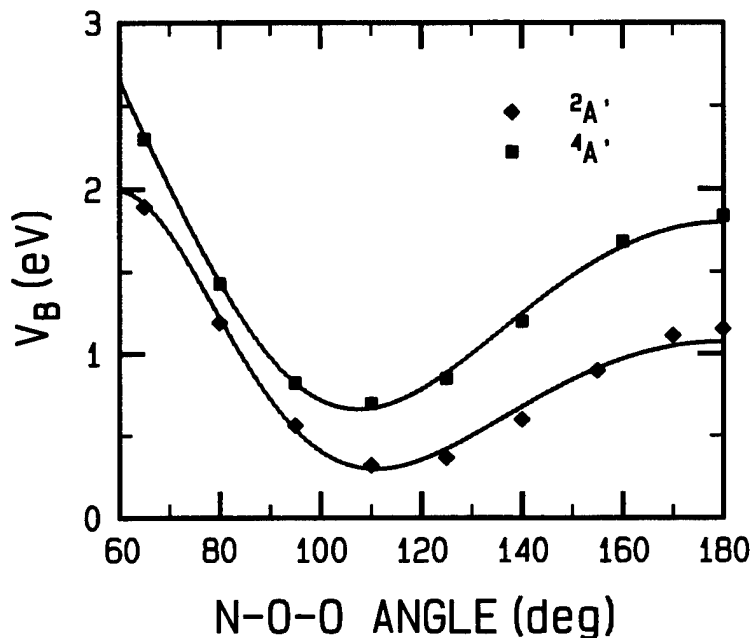


Figure 11. Bending Potentials of the $^2A'$ and $^4A'$ Surfaces in the Region of the Saddle Point. The Solid Lines are the Analytical Fits Using Equation (1) and Filled Symbols are the Adjusted *ab initio* Points.

3.3 Classical Trajectory Methodology

The quasiclassical trajectory (QCT) method⁽⁵⁴⁾ is used to compute the thermal reaction rate constants, and the translational energy dependence of the reaction cross sections and the final vibrational/rotational state distributions. The validity of classical mechanics for calculating reaction rate constants and product distributions has been discussed elsewhere.⁽⁵⁴⁾ Classical calculations are expected to be reliable at energies greater than the barrier heights, where quantum effects such as tunneling may be important, for state-to-state rate constants which are strongly classically allowed. Calculations are carried out separately for the $^2A'$ and $^4A'$ potential energy surfaces and then statistically averaged using the electronic degeneracy factors of 1/6 and 1/3, respectively. Standard Monte Carlo techniques are used to compute the thermal reaction rate constant as a function of temperature, where the translational energy, E_T , and the initial vibrational-rotational states, (v, j) , are chosen from Boltzmann distributions. Cross sections and final $NO(v', j')$ distributions are also calculated as a function of initial translational energy from 0.3 eV to 2.75 eV with the initial (v, j) states selected from a 300 K Boltzmann distribution. The effect of electronic angular momentum on the NO rotational state has been ignored, as the NO

diatomic properties appropriate to the $\text{NO}(X^2\Pi_{1/2})$ ground state have been used. The classical equations of motion are integrated using a variable step size predictor-corrector method.⁽⁵⁵⁾ The final vibrational and rotational quantum numbers (v' , j') are obtained from the correspondence rules $v'_{\text{cl}} = (v' + 1/2)h$ and $j'_{\text{cl}} = (j' + 1/2)\hbar$, where v'_{cl} and j'_{cl} are the classical vibrational and rotational action variables. The final (v' , j') distributions are then obtained using the standard histogram method. A total of 790,000 (540,000 for the $^2A'$ PES and 250,000 for the $^4A'$ PES) trajectories are used in the current study.

3.4 Results and Discussion

3.4.1 Thermal rate constants

Quasiclassical trajectory thermal reaction rate constants are computed for the temperature range of 500 K to 5000 K. A comparison of the calculated thermal rate constant, $k(T)$, with a recommended fit to the available kinetic data⁽⁴³⁾ is shown in Figure 12. The QCT thermal rate constant agrees well with the experimental measurements over the entire temperature range, although the calculations consistently underpredict the rate constants below 1250 K. This systematic disagreement is probably due to two factors: the barrier height of 0.3 eV is either too high, or there is a significant contribution from quantum mechanical tunneling, which cannot be accounted for with the QCT method. Although important for determining low temperature thermal rate constants and the reaction attributes at translational energies near the barrier, neither one of these concerns should be as significant for calculation of the high energy (> 0.5 eV) cross sections and final state distributions reported here. The temperature dependence of the components of the thermal rate constant for the $^2A'$ and $^4A'$ surfaces is shown in Figure 13. As expected, the contribution of $^2A'$ is dominant at temperatures less than 1500 K, due to the lower barrier (0.3 eV) for this surface. The $^4A'$ PES begins to make an important contribution at 2000 K, and is as important as the $^2A'$ surface at 5000 K. This figure illustrates the uncertainty in extrapolating low temperature rate constants to higher temperature, where a significant contribution to the rate constant may come from a mechanism or potential energy surface not important at lower temperatures. In particular, the present calculations indicate that if the lower temperature rate constant (only $^2A'$) is extrapolated to estimate the reaction rate constant at 5000 K, the total rate constant would be underestimated by a factor of 2. The present results are also

in good agreement with the rate constants calculated by Jaffe et al.⁽⁴⁸⁾ using a completely different analytical form for the potential energy surfaces.

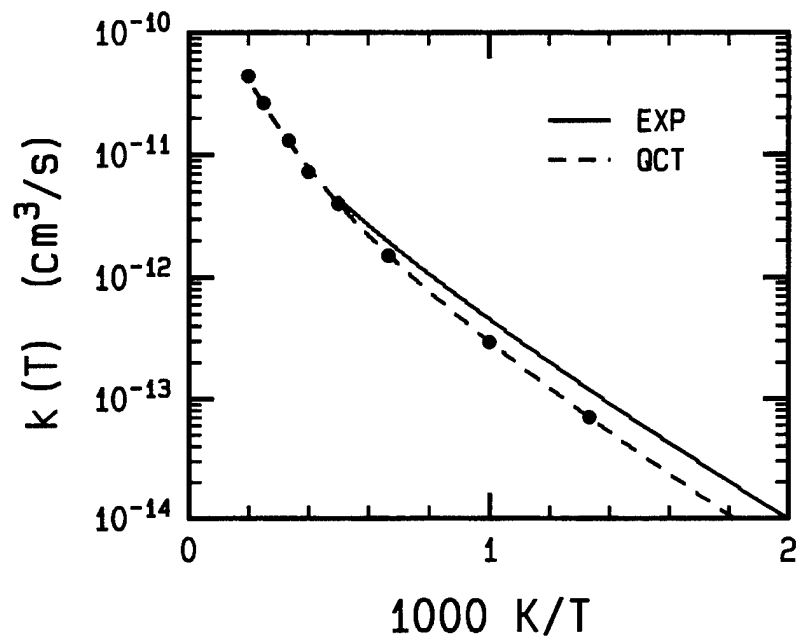


Figure 12. Comparison of the Experimental (—) and QCT(---) Thermal Reaction Rate Constants as a Function of Temperature.

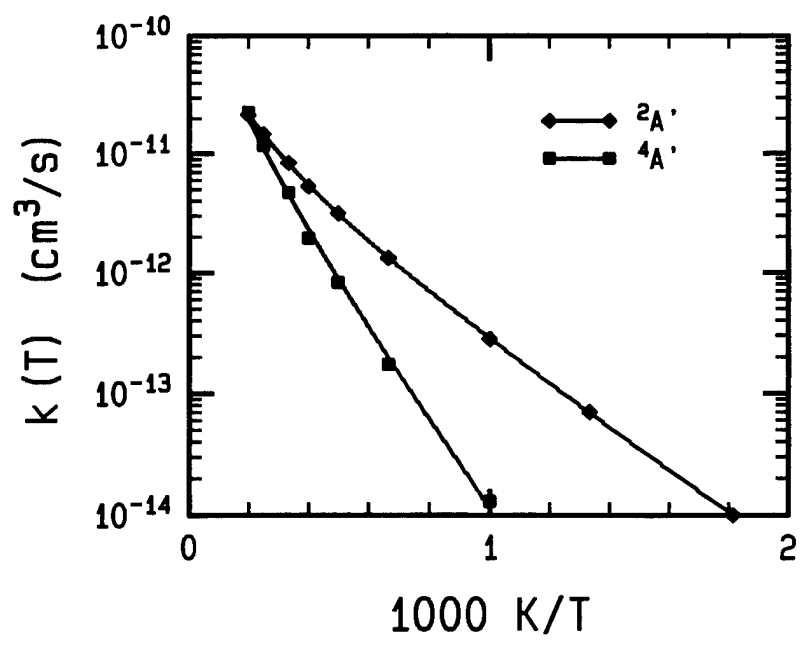


Figure 13. Contributions of the $^2A'$ and $^4A'$ Potential Energy Surfaces to the Thermal Rate Constant.

3.4.2 Energy Dependent Cross Sections

A more useful quantity for the thermospheric NO production models^(10, 35-37) is the reaction cross section as a function of initial translational energy, E_T . Figure 14 shows the total reaction cross section, $\sigma_R(E_T)$, calculated as a function of E_T . Although the initial O_2 vibrational and rotational states were averaged over a Boltzmann distribution at 300 K, the cross sections are insensitive to initial rotational excitation. Also shown in Figure 14 is the individual contribution of the $^2A'$ and $^4A'$ potential energy surfaces to the cross section. Note that the statistical electronic degeneracy factors have been included in the individual cross sections. As expected, the reaction cross section is dominated by the $^2A'$ PES for energies below 1 eV. As the initial translational energy is increased, the relative importance of the $^4A'$ reaction increases and becomes greater than the $^2A'$ reaction above 1.25 eV due to the larger degeneracy factor.

3.4.3 Product Energy Deposition

To assess the possibility of the $N(^4S) + O_2$ reaction contributing to the dayglow NO emission from CIRRIS 1A^(38, 39) and the NO emission from the EXCEDE artificial auroral experiment,⁽⁴¹⁾ it is important to establish the NO vibrational-rotational distributions. The calculated NO vibrational distribution at initial translational energies of 0.5 eV and 1.5 eV is presented in Figure 15. At the lowest translational energy (0.5 eV), the vibrational distribution is relatively flat from $v' = 2$ to $v' = 6$ and then rapidly decreases until the maximum vibrational state ($v' = 9$) is reached. As E_T is increased to 1.5 eV, the maximum vibrational state populated is $v' = 14$. The vibrational distribution peaks around $v' = 4$ and then exponentially decreases until $\sim v' = 12$. The contribution of each PES to the final vibrational distribution at 1.5 eV is shown in Figure 16. Although the vibrational distributions for each PES are normalized to unity, the reaction cross sections are approximately equal at 1.5 eV (Figure 14) and the resultant distribution in Figure 15 is nearly an average of the two distributions. The greater extent of vibrational excitation on the $^2A'$ surface than on the $^4A'$ surface is consistent with the energy release⁽⁵²⁾ and curvature of the minimum energy path⁽⁵³⁾ of the respective surfaces as discussed earlier. The average vibrational quantum numbers at $E_T = 1.5$ eV are 4.6 and 3.4 on the $^2A'$ and $^4A'$ surfaces, respectively.

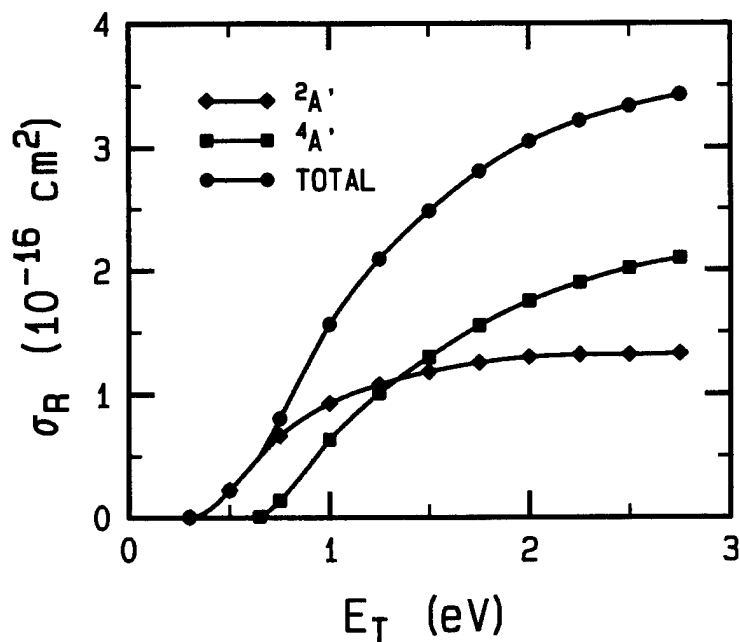


Figure 14. Contribution of the QCT Cross Sections for the $^2A'$ and $^4A'$ Potential Energy Surfaces to the Total Cross Section as a Function of the Initial Relative Translational Energy.

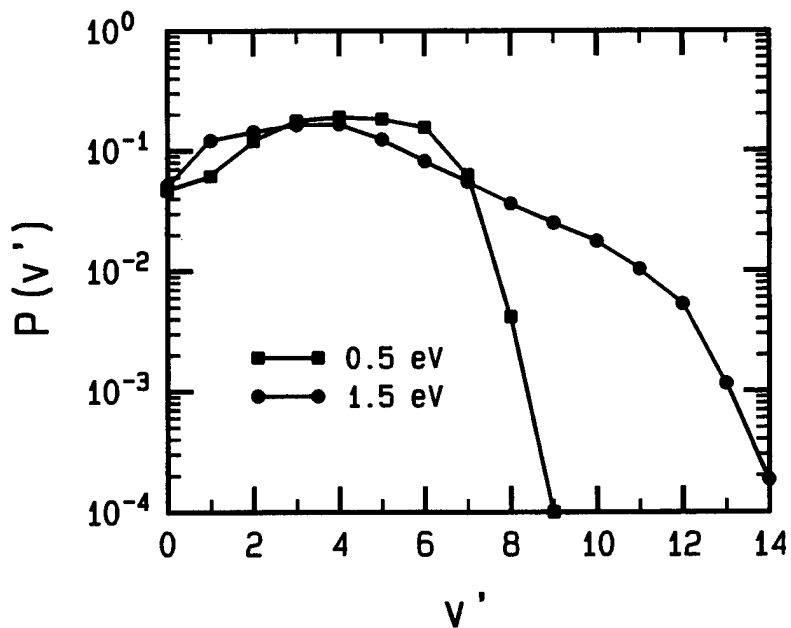


Figure 15. NO Vibrational Distribution as a Function of the Final Vibrational Quantum Number for Initial Relative Translational Energies of 0.5 and 1.5 eV.

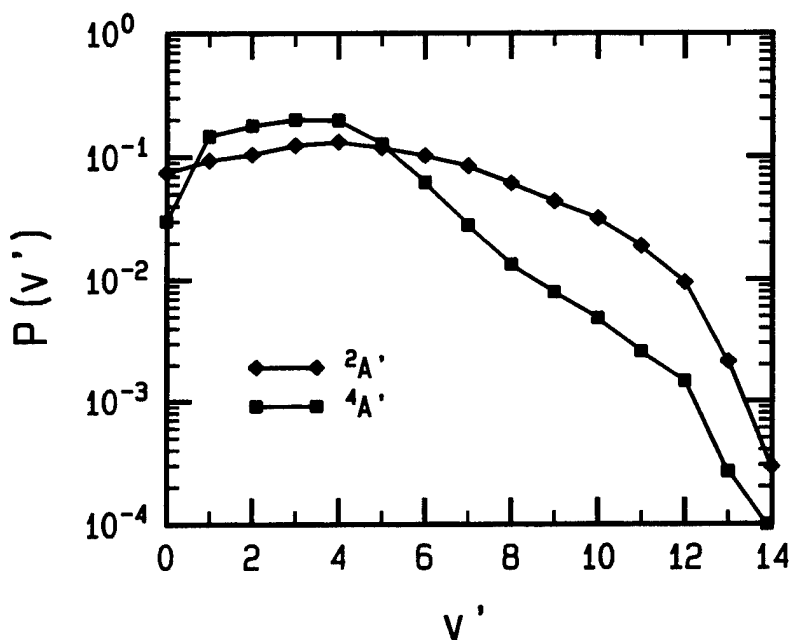


Figure 16. Contribution of the $^2A'$ and $^4A'$ Potential Energy Surfaces to the NO Vibrational Distribution as a Function of the Final Vibrational Quantum Number at an Initial Relative Translational Energy of 1.5 eV.

The present results for the $^2A'$ PES are in qualitative agreement with the calculations of Gilibert et al.,⁽⁴⁰⁾ The largest difference between the calculations is our prediction that the reaction threshold occurs at ~ 0.3 eV, about 0.2 eV lower than the previous calculation. There are also small differences in the NO final vibrational distribution, as the present calculations show that the NO is formed with more energy in vibration. This result is due to the present $^2A'$ PES being more attractive than the surface of Gilibert et al., which is consistent with the *ab initio* calculations.

There have been three previous measurements of the NO vibrational distribution at room temperature.⁽⁴⁴⁻⁴⁶⁾ The measurements of Rahbee and Gibson⁽⁴⁴⁾ fall off exponentially with increasing NO vibrational quantum number in contrast with the $E_T = 0.5$ eV calculation. Herm et al.,⁽⁴⁵⁾ have pointed out the importance of considering the effects of vibrational quenching. The experiment of Herm et al.,⁽⁴⁵⁾ shows a NO vibrational distribution that is qualitatively similar to the QCT distribution at $E_T = 0.5$ eV, although the experiment indicates a substantial population in the $v' = 0$ state. However, again due to vibrational relaxation, it is claimed that the measured distribution only represents a lower bound to the true nascent distribution. An oscillating NO

vibrational distribution was determined in the most recent experiment,⁽⁴⁶⁾ which disagrees with previous measurements. Gilibert et al.,⁽⁴⁹⁾ have attempted to explain qualitatively the oscillations in the vibrational distribution by considering a Franck-Condon model, although their analysis is not conclusive. The present QCT calculations at 0.5 eV indicate that almost 50% of the available energy goes into vibration, somewhat greater than the experimental observation of 24-34%. Thus, the QCT calculations are consistent with the assertion of Herm et al.,⁽⁴⁵⁾ that previous experiments actually measured a partially relaxed vibrational distribution.

Analysis of data from the CIRRIS 1A^(38,39) and EXCEDE III⁽⁴¹⁾ observations have shown that NO is formed in the atmosphere with extensive rotational excitation. If the "hot" $N(^4S) + O_2$ reaction is important in NO formation as indicated by Sharma et al.,⁽⁹⁾ the QCT calculations should show high rotational excitation. The NO rotational distributions, summed over all final vibrational states, are shown in Figure 17 for translational energies of 0.5 eV and 1.5 eV. These distributions are Boltzmann-like with rotational temperatures of 4000 K and 10000 K at translational energies of 0.5 eV and 1.5 eV, respectively. The large amount of NO rotational excitation from the $N(^4S) + O_2$ reaction is in quantitative agreement with the field experiments. The rotational distributions for v' of 1, 4, and 7 are shown in Figure 18, and correspond to rotational temperatures of approximately 16000 K, 9400 K, and 5900 K, respectively. The average rotational quantum number at 0.5 eV and 1.5 eV is shown as a function of vibrational quantum number in Figure 19. The decrease in rotational excitation as the NO vibrational state increases is similar to that expected from a microcanonical rotational distribution. Extensive rotational excitation of NO has also been observed recently by Guadagnini et al.,⁽⁵⁶⁾ in a detailed study of NO formation from a family of HNO reactions.

Lastly, the energy dependence of the energy deposition from the $N(^4S) + O_2$ reaction is presented in Figure 20 as the fraction of the total energy available. At low translational energies, the reaction deposits a large fraction (~60%) of the available energy in vibration, in agreement with many studies of exothermic reactions. As the initial energy increases (and the initial orbital angular momentum), the incremental increase in translational energy is preferentially converted into NO rotational energy, which has been observed, for example, by Muckerman⁽⁵⁷⁾ in the $F + HD$ reaction. This behavior can be qualitatively explained by the spectator stripping model.

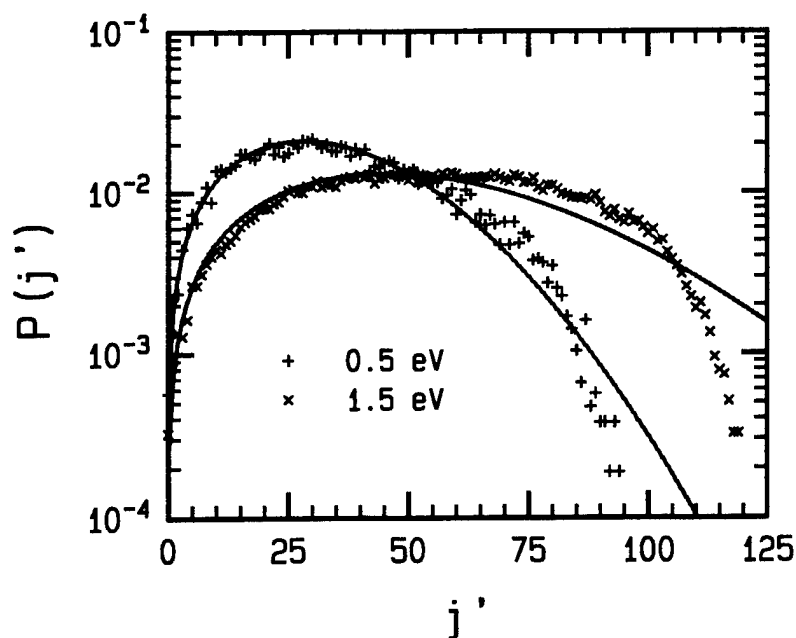


Figure 17. NO Rotational Distribution as a Function of the Final Rotational Quantum Number for Initial Relative Translational Energies of 0.5 and 1.5 eV. The Solid Lines Correspond to Boltzmann Distributions at Rotational Temperatures of 4000 K and 10000 K.

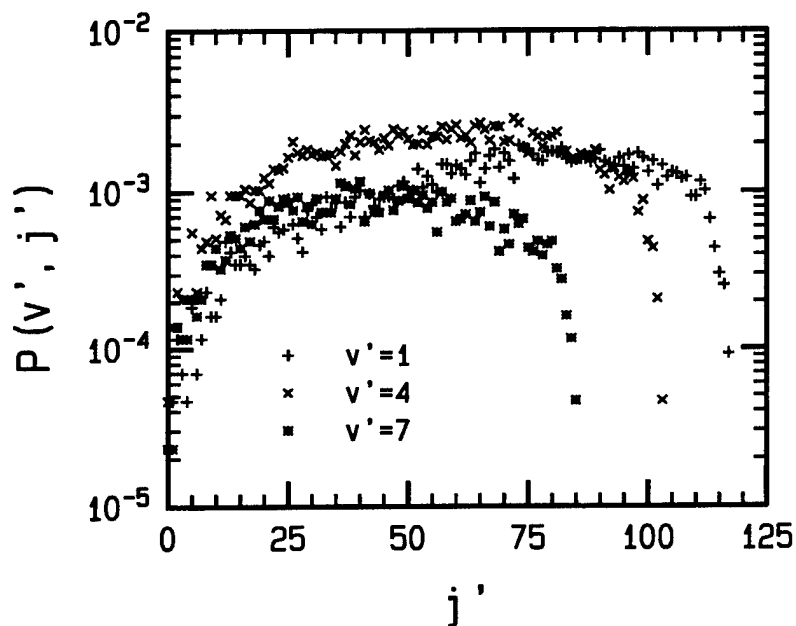


Figure 18. NO Rotational Distribution as a Function of Final Rotational Quantum Number for Several Final Vibrational Quantum Numbers at an Initial Relative Translational Energy of 1.5 eV.

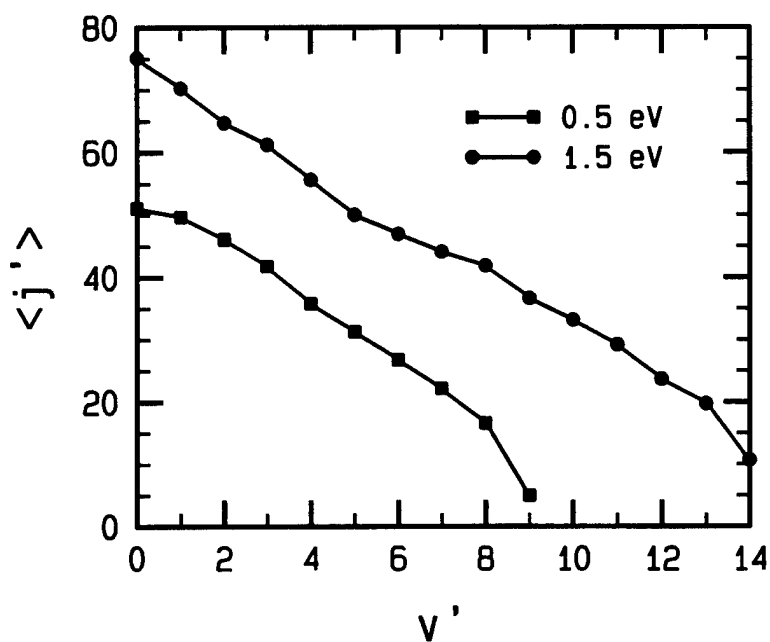


Figure 19. The Average Rotational Quantum Number as a Function of the Final Vibrational Quantum Number at Initial Translational Energies of 0.5 and 1.5 eV.

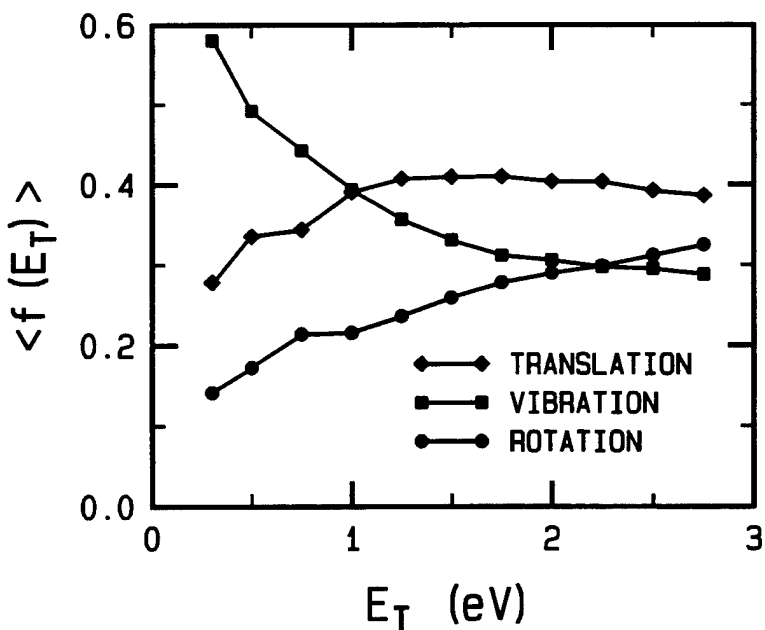


Figure 20. The Fraction of Total Energy in Translation, Vibration, and Rotation for the Reaction Products as a Function of Initial Relative Translational Energy.

3.5 Summary

Extensive quasiclassical trajectory calculations have been performed for the $\text{N}(^4\text{S}) + \text{O}_2(\text{X}^3\Sigma_g^-) \rightarrow \text{NO}(\text{X}^2\Pi) + \text{O}(^3\text{P})$ reaction using realistic *ab initio* potential energy surfaces. The *ab initio* calculations adequately characterized the saddle point region on both the $^2\text{A}'$ and $^4\text{A}'$ electron surfaces, which is important for the determination of the thermal rate constants and energy dependent cross sections. However, the energy release along the minimum energy path, which strongly influences the final NO vibrational distribution, was only established for the $^2\text{A}'$ surface. The reaction attributes were obtained independently on the $^2\text{A}'$ and $^4\text{A}'$ electronic states and statistically averaged using the respective degeneracy factors. Good agreement has been obtained with experimental thermal rate constants, suggesting that the calculations provide a good representation of this reaction. Reaction cross sections and internal NO vibrational-rotational distributions have also been calculated as a function of initial translational energy. The calculated NO vibrational distributions at low translational energy are consistent with available experimental measurements, although the experimental results are colder than the calculated distribution. It has been conjectured that the experimental distributions are partially relaxed. At translational energies greater than 1 eV, the NO vibrational distributions are uncertain due to the increasing influence of the $^4\text{A}'$ surface on the energy disposal. Recent field measurement programs observed NO distributions with extensive vibrational excitation characterized by rotational temperatures on the order of 4000 K to 7000 K,^(39,41) which the present QCT calculations show are consistent with NO formation from the $\text{N}(^4\text{S}) + \text{O}_2$ reaction. Further calculations of NO formation in the atmosphere from translationally hot $\text{N}(^4\text{S}) + \text{O}_2$ using the present results should provide more quantitative evaluation of the relative importance of $\text{N}(^4\text{S})$ as a source of NO in the thermosphere.

4. EVIDENCE FOR NO FORMATION FROM HYPERTHERMAL N(⁴S) ATOMS IN AN ARTIFICIAL AURORAL EXPERIMENT

4.1 Introduction

This section discusses the analysis of electron-beam enhanced NO($\Delta v = 1$) emission observed by the interferometer during EXCEDE III. In addition to considering the traditional N(²D) + O₂ reaction at thermal energies, the chemistry of translationally hot N atoms in NO formation has been investigated in detail, with emphasis on the hyperthermal N(⁴S) + O₂ reaction. It is shown that a quantitative description of rotationally thermal and hot NO emission observed in EXCEDE III requires the inclusion of hyperthermal N atom chemistry in our chemical kinetics model.

Section 2 discusses the evidence for the importance of the reactions of hyperthermal N(⁴S) and N(²D) with O₂ in producing NO. The chemical dynamics of the N(⁴S) + O₂ reaction is discussed in Section 3, and preliminary calculations of NO vibrational populations using a hyperthermal nitrogen atom kinetics model is presented in Section 4.2. A brief summary is given in Section 4.3.

4.2 Chemical Kinetics Model

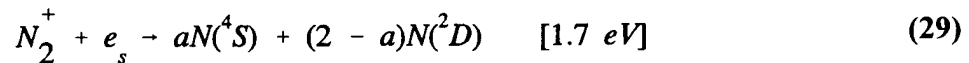
The reactions of metastable nitrogen atoms with molecular oxygen are thought to be the major source of nitric oxide chemiluminescence in the thermosphere.⁽⁵⁾ Earlier models of NO formation assumed that the chemistry of N(²D) is the most significant contributor to NO formation, while the relaxation of N(²P) to N(²D) and the reaction of N(²P) with O₂⁽⁶⁾ make a relatively minor contribution in the thermospheric dayglow⁽³³⁾ and aurora.^(14, 32)

Reaction (1) has previously been considered as a source of rotationally thermal NO.^(7, 8) The production mechanism of rotationally hot NO is currently unknown, although it has been suggested that the reaction of N(²P) with O₂ is a possible source.⁽⁸⁾ However, it has been shown (J. W. Duff, unpublished work, 1994) that Reaction (2) can not be a significant source of rotationally thermal or hot NO emission under the conditions of the EXCEDE III experiment.

Further evidence of the inadequacy of Reaction (1) is provided by the analysis of the interferometer data at apogee which shows significant emission from highly rotationally excited

NO. At apogee, Reaction (1) does not produce the correct NO vibrational distribution to explain the rotationally thermal populations obtained from the interferometer data. Recently, it has been suggested that the reaction of translationally hot $N^*(^4S)$ with O_2 may be an important contributor to NO formation in the thermosphere.^(34, 36) Furthermore,⁽⁹⁾ have argued the importance of the $N^*(^4S) + O_2$ reaction in recent observations of highly rotationally excited NO vibrational emissions in the dayglow.^(38, 39)

In order to assess the importance of Reaction (3) as a significant source of NO which is both highly rotationally and vibrationally excited in EXCEDE III, we have created a time-dependent kinetics model incorporating a mechanism for producing NO from "hot" $N^*(^4S)$. The most important inputs for this model are the reaction cross section for the $N^*(^4S) + O_2 \rightarrow NO(v,j) + O$ process, and the quenching of $N^*(^4S)$ by major atmospheric species. The model used for the quenching of $N^*(^4S)$ is similar to that used by Logan and McElroy in the study of fast oxygen atoms.⁽⁵⁸⁾ The translational energy distribution function for the $N^*(^4S) + O_2$ reaction is defined in the energy range 0 - 1.5 eV. This energy range is subdivided into finite bins of width 0.1 eV. The reaction rate constants for $N^*(^4S) + O_2$ from the quasiclassical trajectory calculations are then computed at a translational energy corresponding to the average energy of each bin. The various sources, and associated translational energy, of $N^*(^4S)$ from irradiation of the atmosphere are





The translational energies from Reactions (28) - (35) are transformed to the $N(^4S) + O_2$ center of mass and placed in the appropriate energy bin. There are estimates of the cross section for the quenching of $N(^4S)$, although the uncertainties are unknown. We have chosen a reasonable value of $5 \times 10^{-16} \text{ cm}^2$ for



which is to be compared with the gas kinetic estimate of $3 \times 10^{-15} \text{ cm}^2$.

The rotationally hot vibrational populations calculated from Reaction (3) are compared to the NO populations obtained from the interferometer data⁽⁵⁹⁾ at an altitude of 103 km (upleg) in Figure 21. The excellent agreement between the chemical kinetics model and data provide the first quantitative evidence that Reaction (3) is the source of rotationally hot NO in disturbed atmospheres. Also shown in Figure 21 is a comparison of the vibrational populations obtained from Reaction (1) using the nascent vibrational distribution of Kennealy et al.,⁽⁷⁾ with the rotationally thermal populations from the interferometer. Again the agreement of the kinetics model and the data is excellent, indicating that the $N(^2D)$ is thermalized at 103 km (upleg).

A similar comparison of the rotationally thermal and hot NO vibrational populations from the model and interferometer data at 115 km (apogee) is shown in Figure 22. For the thermal rotational component, the vibrational populations from the kinetic model are approximately a factor of 3 below the data. This comparison implies that the $N(^2D)$ is probably not thermalized at 115 km, and the rate constant and vibrational distribution used for Reaction (1) is not correct. Figure 22 also contains a comparison of the rotationally hot vibrational populations from Reaction (3) with the interferometer data. Although the kinetic model is in reasonable agreement with the data, the model underpredicts the vibrational populations for low vibrational quantum numbers. At this altitude (115 km), $N(^4S)$ translational energies in the range of 1 to 2 eV is most important for producing NO. As is evident from Figure 14 in Section 3, the $^4A'$ PES makes a significant contribution to the NO vibrational distribution. Unfortunately, the regions of the PES which are most important for determining the vibrational distribution on the $^4A'$ PES are not available from the *ab initio* calculations. Evidently the $^4A'$ PES is more repulsive (i.e., colder NO vibrational distribution) than the PES used in Section 3. Testing of this hypothesis will have to await more extensive *ab initio* calculations.

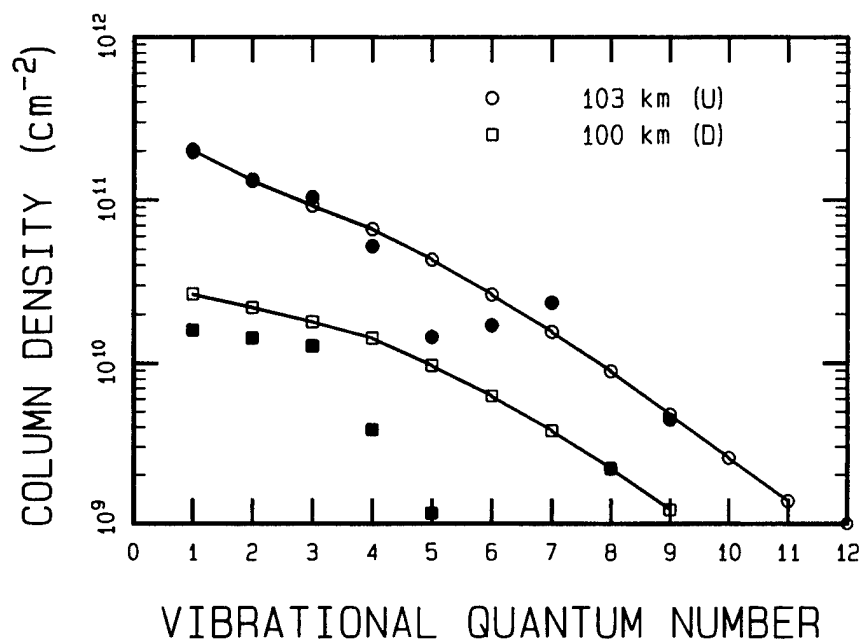


Figure 21. Comparison of the NO Vibrational Populations for the Rotationally hot Component Derived from the Interferometer Data at an Altitude of 103 km During Upleg with the EXCEDE Kinetic Model Using the $N^*(^4S) + O_2$ Mechanism.

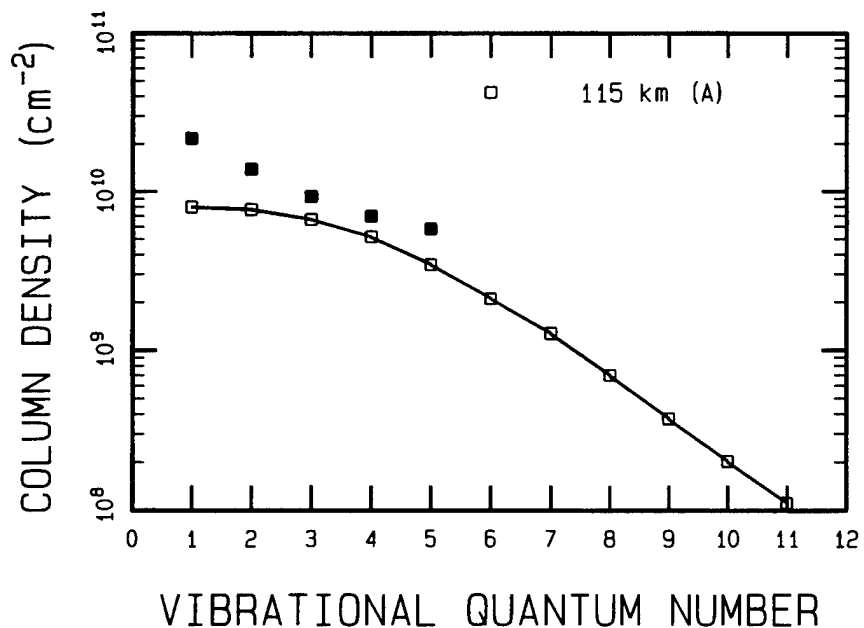


Figure 22. Same as Figure 21 Except for an Altitude of 115 km (apogee).

4.3 Summary

This analysis has provided the first quantitative evidence of the importance of hyperthermal $N(^4S)$ and $N(^2D)$ atoms in the formation of vibrationally and rotationally excited NO. The rate constants and vibrational distributions for rotationally hot NO are obtained from extensive quasiclassical trajectory calculations for the $N(^4S) + O_2(X^3\Sigma_g^-) \rightarrow NO(X^2\Pi) + O(^3P)$ reaction using realistic *ab initio* potential energy surfaces. Good agreement has been obtained with experimental thermal rate constants, indicating that the calculations are a good representation of this reaction. Reaction rate constants and internal NO vibrational-rotational distributions have also been calculated as a function of initial translational energy. The NO vibrational-rotational distributions at low translational energy are consistent with available experimental measurements. Recent field measurement programs observed NO distributions with extensive vibrational excitation characterized by rotational temperatures on the order of 4000 K to 7000 K,^(39, 41) which the present QCT calculations show are consistent with NO formation from the $N(^4S) + O_2$ reaction.

Quantitative agreement between the chemical kinetics model developed for EXCEDE and the vibrational populations derived from the interferometer data is obtained under conditions of thermalization of nitrogen atoms (i.e., at 103 km under max dose conditions). Analysis of the vibrational populations from the interferometer under other conditions indicate that either hyperthermal $N(^2D)$ atoms also play an important role in NO formation and/or additional mechanism(s) are important. Information concerning the $N(^2D) + O_2$ reaction at hyperthermal translational energies, analogous to that obtained in the present work for the $N(^4S) + O_2$ reaction, is not currently available.

The results of this study indicate that a quantitative understanding of NO formation in the thermosphere will require a detailed investigation into the dynamics of $N(^2D) + O_2$ reaction. Limited *ab initio* studies of the $N(^2D) + O_2$ system have been carried out to characterize the reaction pathways.⁽⁶⁰⁾ Although a total of five potential energy surfaces will have to be considered to treat the dynamics of $N(^2D) + O_2$, the calculations are well within the scope of the quasiclassical trajectory method discussed in this report. Given a more extensive and well chosen

set of *ab initio* points for the PES than is currently available, such calculations for this system could be pursued in the future.

5. SUMMARY

The EXCEDE III experiment has provided quantitative characterization of the $N(^2D)$ 5200 Å, the $N(^2P)$ 3466 Å, and the $NO(\Delta v=1$ and $\Delta v=2)$ emissions resulting from the irradiation of the lower thermosphere (90 - 115 km) by an intense electron beam. A detailed chemical kinetics model has been developed describing the interaction of an electron beam with the atmosphere including the geometry of the EXCEDE III measurement. The model indicates that the $N(^2D)$ emission can be quantitatively explained by assuming accepted production rates of $N(^2D)$ and N_2^+ created by the electron beam dissociation, consistent with previous auroral models. Using the previous estimate of 0.22 $N(^2P)$ per ion pair⁽¹⁴⁾ from electron dissociation of N_2 results in a model prediction which is approximately 50% below the data, in disagreement with previous analyses of $N(^2P)$ auroral and dayglow emission.^(14,32,33) However, it should be recalled that the EXCEDE III measurement of $N(^2P)$ was not made under steady state conditions, which are appropriate to the atmospheric observations. The present analysis would imply that the amount of $N(^2P)$ from N_2 dissociation should be about a factor of 2 greater than previously assumed or an additional source of $N(^2P)$ exists for intense electron beams such as that used in EXCEDE III.

To assess the contribution of the nonthermal $N(^4S)$ to NO production, extensive quasiclassical trajectory calculations have been performed for the $N(^4S) + O_2(X^3\Sigma_g^-) \rightarrow NO(X^2\Pi) + O(^3P)$ reaction using realistic *ab initio* potential energy surfaces. Good agreement has been obtained with experimental thermal rate constants, suggesting that the calculations provide a good representation of this reaction. Reaction cross sections and internal NO vibrational-rotational distributions have also been calculated as a function of initial translational energy. Recent field measurement programs observed NO distributions with extensive vibrational excitation characterized by rotational temperatures on the order of 4000 K to 7000 K,^(39,41) which the present QCT calculations show are consistent with NO formation from the $N(^4S) + O_2$ reaction.

The first evidence of the importance of hyperthermal $N(^4S)$ and $N(^2D)$ atoms in the formation of vibrationally and rotationally excited NO is described in this report. The rate constants and vibrational distributions for rotationally hot NO are obtained from the quasiclassical trajectory calculations for the $N(^4S) + O_2(X^3\Sigma_g^-)$ discussed in Section 3. Quantitative agreement between the chemical kinetics model and the vibrational populations derived from the interferometer data is obtained under conditions of thermalization of nitrogen atoms (i.e., at 103 km under max dose

conditions). Analysis of the vibrational populations from the interferometer under other conditions at apogee indicate that either hyperthermal $N(^2D)$ atoms also play an important role in NO formation and/or additional mechanism(s) need to be considered.

6. REFERENCES

1. S. A. Rappaport, R. J. Rieder, W. P. Reidy, R. L. McNutt, Jr., J. J. Atkinson, and D. E. Paulsen, "Remote X Ray Measurements Of The Electron Beam From The EXCEDE III Experiment," *J. Geophys. Res.*, **98**, 19093-19098 (1993).
2. R. J. Reider, R. L. McNutt, S. A. Rappaport, "Characterization Of The Energy Deposition Produced By The Primary Electron Beam On The EXCEDE III Experiment," *Visidyne Rep. VI-2067*, **32** pp., Visidyne, Inc., Burlington, MA (1993), PL-TR-93-2132(I), ADA274453.
3. O. Ashihara and K. Takayanagi, "Velocity Distribution Of Ionospheric Low-Energy Electrons," *Planet. Space Sci.*, **22**, 1201-1217 (1974).
4. M. Martinez-Sanchez, W. Cheng, D. Dvornak, and M. S. Zahniser, "Electron Energy Distribution From Intense Electron Beams In The Upper Mesosphere And Lower Thermosphere," *J. Geophys. Res.*, **97**, 1363-1375 (1992).
5. J.-C. Gérard, "Thermospheric Odd Nitrogen," *Planet. Space Sci.*, **40**, 337-353 (1992).
6. L. G. Piper, "The Reactions Of $N(^2P)$ With O_2 And O ," *J. Chem. Phys.*, **98**, 8560-8564 (1993).
7. J. P. Kennealy, F. P. Del Greco, G. E. Caledonia, and B. D. Green, "Nitric Oxide Chemiexcitation Occurring In The Reaction Between Metastable Nitrogen Atoms And Oxygen Molecules," *J. Chem. Phys.*, **69**, 1574-1584 (1978).
8. W. T. Rawlins, M. E. Fraser, and S. M. Miller, "Rovibrational Excitation Of Nitric Oxide In The Reaction Of O_2 With Metastable Atomic Nitrogen," *J. Phys. Chem.*, **93**, 1097-1107 (1989).
9. R. D. Sharma, Y. Sun, and A. Dalgarno, "Highly Rotationally Excited Nitric Oxide In The Terrestrial Thermosphere," *Geophys. Res. Letters*, **20**, 2043-2045 (1993).
10. V. I. Shematovich, D. V. Bisikalo, and J. C. Gérard, "Non Thermal Nitrogen Atoms In The Earth's Thermosphere 1. Kinetics Of Hot $N(^4S)$," *Geophys. Res. Lett.*, **18**, 1691-1694 (1991).
11. J. W. Duff, F. Bien, and D. E. Paulsen, "Classical Dynamics Of The $N(^4S)+O_2(X^3\Sigma_g^-)\rightarrow NO(X^2\Pi)+O(^3P)$ Reaction," *Geophys. Res. Lett.*, **21**, 2043-2046 (1994).
12. H. S. Porter, C. H. Jackman, and A. E. S. Green, "Efficiencies For Production Of Atomic Nitrogen And Oxygen By Relativistic Proton Impact In Air," *J. Chem. Phys.*, **65**, 154-167 (1976).
13. D. W. Rusch, J.-C. Gérard, S. Solomon, P. J. Crutzen, and G. C. Reid, "The Effect Of Particle Precipitation Events On The Neutral And Ion Chemistry Of The Middle Atmosphere-I. Odd Nitrogen," *Planet. Space Sci.*, **29**, 767-774 (1981).

14. E. C. Zipf, P. J. Espy, and C. F. Boyle, "The Excitation And Collisional Deactivation Of Metastable $N(^2P)$ Atoms In Auroras," *J. Geophys. Res.*, **85**, 687-694 (1980).
15. D. Rapp, P. Englander-Golden, and D. D. Briglia, "Cross Sections For Dissociative Ionization Of Molecules By Electron Impact," *J. Chem. Phys.*, **42**, 4081-4085 (1965).
16. F. J. Mehr and M. A. Biondi, "Electron Temperature Dependence Of Recombination Of O_2^+ And N_2^+ Ions With Electrons," *Phys. Rev.*, **181**, 264-271 (1969).
17. E. Alge, N. G. Adams, and D. Smith, "Measurements Of The Dissociative Recombination Coefficients Of O_2^+ , NO^+ , And NH_4^+ In The Temperature Range 200-600 K," *J. Phys. B: At. Mol. Phys.*, **16**, 1433-1444 (1983).
18. J. L. Queffelec, B. R. Rowe, M. Morlais, J. C. Gomet, and F. Vallee, "The Dissociative Recombination Of $N_2^+(v=0,1)$ As A Source Of Metastable Atoms In Planetary Atmospheres," *Planet. Space Sci.*, **33**, 263-270 (1985).
19. D. Kley, G. M. Lawrence, and E. J. Stone, "The Yield Of $N(^2D)$ Atoms In The Dissociative Recombination Of NO^+ ," *J. Chem. Phys.*, **66**, 4157-4165 (1977).
20. D. L. McFarland, D. L. Albritton, F. C. Fehsenfeld, E. E. Ferguson, and A. L. Schmeltekopf, "Energy Dependence And Branching Ratio Of The $N_2^+ + O$ Reaction," *J. Geophys. Res.*, **79**, 2925-2926 (1974).
21. D. Smith, N. G. Adams, and T. M. Miller, "A Laboratory Study Of The Reactions Of N^+ , N_2^+ , N_3^+ , N_4^+ , O^+ , O_2^+ , And NO^+ Ions With Several Molecules At 300 K," *J. Chem. Phys.*, **69**, 308-318 (1978).
22. M. A. Smith, V. M. Bierbaum, and S. R. Leone, "Infrared Chemiluminescence From Vibrationally Excited NO^+ : Product Branching In The $N^+ + O_2$ Ion-Molecule Reaction," *Chem. Phys. Letters*, **94**, 398-403 (1983).
23. C. Fell, J. I. Steinfeld, and S. Miller, "Quenching Of $N(^2D)$ By $O(^3P)$," *J. Chem. Phys.*, **92**, 4768-4777 (1990).
24. K. A. Berrington and P. G. Burke, "Effective Collision Strengths For Forbidden Transitions In e-N And e-O Scattering," *Planet. Space Sci.*, **29**, 377-381 (1981).
25. C. B. Opal, W. K. Peterson, and E. C. Beaty, "Measurements Of Secondary-Electron Spectra Produced By Electron Impact Ionization Of A Number Of Simple Gases," *J. Chem. Phys.*, **55**, 4100-4106 (1976).
26. M. H. Rees and R. A. Jones, "Time Dependent Studies Of The Aurora-II. Spectroscopic Morphology," *Planet. Space Sci.*, **21**, 1213-1235 (1971).
27. Y. Itikawa, M. Hayashi, A. Ichimura, K. Onda, K. Sakimoto, K. Takayanagi, M. Nakamura, H. Nishimura, and T. Takayanagi, "Cross Sections For Collisions Of Electrons And Photons With Nitrogen Molecules," *J. Phys. Chem. Ref. Data*, **15**, 985-1010 (1986).

28. Y. Itikawa, A. Ichimura, K. Onda, K. Sakimoto, K. Takayanagi, Y. Hatano, M. Hayashi, H. Nishimura, and S. Tsurubuchi, "Cross Sections For Collisions Of Electrons And Photons With Oxygen Molecules," *J. Phys. Chem. Ref. Data*, **18**, 23-42 (1989).
29. Y. Itikawa and A. Ichimura, "Cross Sections For Collisions Of Electrons And Photons With Atomic Oxygen," *J. Phys. Chem. Ref. Data*, **19**, 637-651 (1990).
30. C. W. Gear, *Numerical Initial Value Problems in Ordinary Differential Equations*, Prentice-Hall, Englewood Cliffs, NJ (1971).
31. A. E. Hedin, "Extension Of The MSIS Thermosphere Model Into The Middle And Lower Atmosphere," *J. Geophys. Res.*, **96**, 1159-1172 (1991).
32. J.-C. Gérard and O. E. Harang, "Metastable N(²P) Atoms In The Aurora," *J. Geophys. Res.*, **85**, 1757-1761 (1980).
33. M. R. Torr, D. G. Torr, and P. G. Richards, "N(²P) In The Dayglow: Measurement And Theory," *Geophys. Res. Lett.*, **20**, 531-534 (1993).
34. S. Solomon, "The Possible Effects of Translationally Excited Nitrogen Atoms on Lower Thermospheric Odd Nitrogen," *Planet. Space Sci.*, **31**, 135-139 (1983).
35. Ø. Lie-Svendsen, M. H. Rees, K. Stamnes, and E. C. Whipple, Jr., "The Kinetics of "Hot" Nitrogen Atoms in Upper Atmosphere Neutral Chemistry," *Planet. Space Sci.*, **39**, 929-943 (1991).
36. V. I. Shematovich, D. V. Bisikalo, and J.-C. Gérard, "The Thermospheric Odd Nitrogen Photochemistry: Role of Non Thermal N(⁴S) Atoms," *Ann. Geophysicae*, **10**, 792-801 (1992).
37. R. D. Sharma, V. A. Kharchenko, Y. Sun, and A. Dalgarno, "Energy Distribution of Fast Nitrogen Atoms in the Nighttime Terrestrial Thermosphere," *J. Geophys. Res.*, **101**, 275-281 (1996).
38. D. R. Smith and M. Ahmadjian, "Observation of Nitric Oxide Rovibrational Band Head Emissions in the Quiescent Airlow by the CIRRIS-1A Space Shuttle Experiment," *Geophys. Res. Lett.*, **20**, 2679-2682 (1993).
39. P. S. Armstrong, S. J. Lipson, J. A. Dodd, J. R. Lowell, W. A. M. Blumberg, and R. M. Nadile, "Highly Rotationally Excited NO(v,J) in the Thermosphere from CIRRIS 1A Limb Radiance Measurements," *Geophys. Res. Lett.*, **21**, 2425-2428 (1994).
40. M. Gilibert, A. Aguilar, M. González, and R. Sayós, "Quasiclassical Trajectory Study of the N(⁴S_u) + O₂(X³Σ_g⁻) → NO(X²Π) + O(³P_g) Atmospheric Reaction on the ²A' Ground Potential Energy Surface Employing an Analytical Sorbie-Murrell Potential," *Chem. Phys.*, **172**, 99-115 (1993).
41. S. J. Lipson, P. S. Armstrong, J. R. Lowell, W. A. M. Blumberg, D. E. Paulsen, M. J. Fraser, W. T. Rawlins, B. D. Green, R. E. Murphy, and J. A. Dodd, "Mission-Wide EXCEDE III Nitric Oxide Spectroscopic Analysis (abstract)," *Eos Trans. AGU*, **74**, 225, 1993.

42. S. P. Walch and R. L. Jaffe, "Calculated Potential Surfaces for the Reactions: $O+N_2 \rightarrow NO+N$ and $N+O_2 \rightarrow NO+O$," *J. Chem. Phys.*, **86**, 6946-6956 (1987).
43. D. L. Baulch, D. D. Drysdale, and D. G. Haine, *Evaluated Kinetic Data for High Temperature Reactions*, **2**, Butterworths, London (1973).
44. A. Rahbee and J. J. Gibson, "Rate Constants for Formation of NO in Vibrational Levels $v=2$ Through 7 From the Reaction $N(^4S)+O_2 \rightarrow NO^{\dagger}+O$," *J. Chem. Phys.*, **74**, 5143-5148 (1981).
45. R. R. Herm, B. J. Sullivan, and M. E. Whitson, Jr., "Nitric Oxide Vibrational Excitation From the $N(^4S)+O_2$ Reaction," *J. Chem. Phys.*, **79**, 2221-2230 (1983).
46. I. C. Winkler, R. A. Stachnik, J. I. Steinfeld, and S. M. Miller, "Determination of $NO(v=0-7)$ Product Distribution From the $N(^4S)+O_2$ Reaction Using Two-Photon Ionization," *J. Chem. Phys.*, **85**, 890-899 (1988).
47. G. E. Caledonia, Private Communication, Physical Sciences, Inc., November, 1993.
48. R. L. Jaffe, M. Pattengill, and D. W. Schwenke, "Classical Trajectory Studies of Gas Phase Reaction Dynamics and Kinetics Using *ab initio* Potential Energy Surfaces," in *Supercomputer Algorithms for Reactivity, Dynamics, and Kinetics of Small Molecules*, edited by A. Laganá, pp. 367-382, Kluwer, Dordrecht (1989).
49. M. Gilibert, X. Giménez, M. González, R. Sayós, and A. Aguilar, "A Comparison between Experimental, Quantum and Quasiclassical Properties for the $N(^4S)+O_2(X^3\Sigma_g^-) \rightarrow N_2(X^2\Pi)+O(^3P)$ Reaction," *Chem. Phys.*, **191**, 1-11 (1995).
50. K. S. Sorbie and J. N. Murrell, "Analytical Potentials for Triatomic Molecules from Spectroscopic Data," *Mol. Phys.*, **29**, 1387-1407 (1975).
51. J. N. Murrell and K. S. Sorbie, "New Analytic Form for the Potential Energy Curves of Stable Diatomic States," *J. Chem. Soc. Faraday Trans.*, **70**, 1552-1556 (1974).
52. P. J. Kuntz, E. M. Nemeth, J. C. Polanyi, S. D. Rosner, and C. E. "Energy Distribution Among Products of Exothermic Reactions. II. Repulsive, Mixed, and Attractive Energy Release," *J. Chem. Phys.*, **44**, 1168-1184 (1966).
53. J. W. Duff and D. G. Truhlar, "Effect of curvature of the reaction path on dynamic effects in endothermic chemical reactions and product energies in exothermic reactions," *J. Chem. Phys.*, **62**, 2477-2491 (1975).
54. D. G. Truhlar and J. T. Muckerman, "Reactive Scattering Cross Sections III: Quasiclassical and Semiclassical Methods," in *Atom-Molecule Collision Theory*, edited by R. B. Bernstein, pp. 505-566, Plenum, New York (1979).
55. P. Brumer, "Stability Concepts in the Numerical Solution of Classical Atomic and Molecular Scattering Problems," *J. Comp. Phys.*, **14**, 391-419 (1974).
56. R. Guadagnini, G. C. Schatz, and S. P. Walch, "Quasiclassical Trajectory Studies of $N+OH$, $O+NH$, and $H+NO$ Collisions Using Global *ab initio* Potential Energy Surfaces," *J. Chem. Phys.*, **102**, 784-791 (1995).

57. J. T. Muckerman, "Classical Dynamics of the Reaction of Fluorine Atoms with Hydrogen Molecules. III. The Hot-Atom Reactions of ^{16}F with HD^* ," *J. Chem. Phys.*, **57**, 3388-3396 (1972).
58. J. A. Logan and M. B. McElroy, "Distribution Functions for Energetic Oxygen Atoms in the Earth's Lower Atmosphere," *Planet. Space Sci.*, **25**, 117-122 (1977).
59. M.E. Fraser, W. T. Rawlins, and B. D. Green, Private Communication, Physical Sciences, Inc., February, 1994.
60. H.H. Michels, "Theoretical Research Investigation for Air Molecular Calculations, Report No. AFGL-TR-81-0151 (April, 1981). ADA112286